Research Article

Robust Approximation for Non-Linear Variable-Distributed Fractional Differential Equation with Non-Smooth Solutions

A. Emin[1], M. A. Abdelkawy[2*] (ID), Anjan Biswas[3,4,5,6] (ID)

[1] Department of Software Engineering, Istanbul Gelisim University, Istanbul, 34310, Turkey
[2] Department of Mathematics and Statistics, College of Science, Imam Mohammad Ibn Saud Islamic University (IMSIU), Riyadh, Saudi Arabia
[3] Department of Mathematics and Physics, Grambling State University, Grambling, LA, 71245-2715, USA
[4] Department of Physics and Electronics, Khazar University, Baku, AZ, 1096, Azerbaijan
[5] Department of Applied Sciences, Cross-Border Faculty of Humanities, Economics and Engineering Dunarea de Jos University of Galati, 111 Domneasca Street, Galati, 800201, Romania
[6] Department of Mathematics and Applied Mathematics, Sefako Makgatho Health Sciences University Medunsa, 0204, Pretoria, South Africa
 E-mail: maohamed@imamu.edu.sa

Abstract: This article introduces a spectral method aimed at estimating solutions for nonlinear Variable Distributed-Order Fractional Differential Equations (VDO-FDEs) with a non-smooth solution in one-dimensional and time-nonlinear VDO-FDEs. Initially, we express the solution and its fractional derivatives using a series of Shifted Legendre Polynomials (SLPs). Subsequently, the expansion coefficients were derived by transforming the VDO-FDEs in addition to the conditions related to the algebraic system. We illustrate effectiveness and feasibility through various numerical tests.

1. Introduction

Fractional Differential Equations (FDEs) [1, 2] find wide application in various fields due to being able to simulate complicated memory-related phenomena, hereditary properties, and non-local effects. One prominent application of FDEs is in physics [3, 4]. For example, FDEs are used to characterize the performance of materials with properties that change over time like creep and relaxation. In engineering, FDEs are employed in control theory to design controllers for systems with fractional-order dynamics [5], leading to improved performance and stability. Additionally, FDEs play a crucial role in modeling biological processes [6] such as population dynamics, cell growth, and drug transport in tissues, where the non-local and memory effects captured by fractional calculus are essential for accurate predictions and analysis. Furthermore, FDEs have applications in finance for modeling complex market behaviors [7] and in signal processing for analyzing signals with long-term dependencies and non-local correlations [8]. The authors in [9, 10] analyzed quantum

information entropy in hyperbolic potentials within the fractional Schrödinger equation and showed that decreasing the fractional derivative enhanced position-space localization while increasing momentum-space delocalization, with key entropy inequalities and Fisher information trends validated while in [11] further demonstrated that these effects persisted in double well potentials, with the BBM inequality satisfied and Fisher entropy increasing with potential depth.

Rabiei and Razzaghi in [12] introduced fractional Boubaker wavelets to solve Fractional Riccati Differential Equations (FRDEs), while the author in [13] introduced fractional-order generalized Legendre wavelets and applied them to solve FRDEs by utilizing the hypergeometric function. Doha et al. in [14] presented a spectral method for approximating the variable-order FRDEs by utilizing shifted Chebyshev polynomial series to expand the solution. The author in [15] implemented a numerical method, the iterative reproducing-kernel algorithm, for solving FRDEs. Tvyordyj [16] investigated the FRDEs with a variable fractional derivative, reflecting the medium's hereditary property and its dependence on past states and develop Numerical Solution of a FRDEs by employing finite differences for appreciating the variable-order derivative and solving the resulting non-linear algebraic system. The author in [17] introduced a Galerkin Mittag-Leffler method with a derived Riemann-Liouville operational matrix to efficiently solve multi-dimensional fractional optimal control problems, while in [18] presented fractional-order Alpert multiwavelet functions and a Riemann-Liouville operational matrix to efficiently solve fractional pantograph differential equations by reducing them to algebraic systems with proven error analysis and validated examples.

Variable-Distributed Order Fractional Riccati Differential Equations (VDO-FDEs) with non-smooth solutions represent a challenging and important area of mathematical modeling. These equations go beyond classical Riccati equations by incorporating fractional derivatives of variable order and a distribution of memory effects. This allows them to describe a wider range of phenomena where both the order of differentiation and the "memory" of the system vary. The analysis of VDO-FDEs with non-smooth solutions remains highly challenging. Traditional methods for solving Riccati equations often fail when applied to variable-distributed order problems, due to the complexity introduced by fractional derivatives

For four decades, spectral approaches have been widely used in various fields, as highlighted by [19–23]. Fourier-expanded spectrum approaches, which were initially used in constrained contexts such as periodic boundary conditions and fundamental geometries, have recently experienced substantial theoretical advances, allowing them to provide effective solutions to multifarious issues. In comparison to other numerical approaches, spectral procedures outperform them in terms of accuracy and exponential convergence rates. All spectral approaches rely on representing solutions as a finite series of orthogonal functions. Several spectral approaches exist, including collocation [24–27], tau [28–30], Galerkin [31], and Petrov-Galerkin [32, 33], where coefficients are optimized to minimize absolute errors. Spectral collocation, for example, approximates differential equation solutions nearly perfectly, allowing residuals to approach zero at specific points.

The spectral method, while highly accurate for smooth problems, faces several limitations when applied to nonlinear or higher-dimensional problems. The computational cost increases significantly due to dense system matrices and the need for iterative solvers for nonlinear terms. In higher dimensions, the number of basis functions grows rapidly, leading to memory and scalability challenges. Moreover, strong nonlinearities can introduce aliasing errors, and complex geometries require additional mapping or domain decomposition, reducing efficiency. Finally, time-dependent problems may face stability constraints, necessitating careful selection of time-stepping schemes. The approach utilizes fractional Shifted Legendre Gauss-Lobatto (SL-GL) point to approximate solutions for non-linear VDO-FDEs, with non-smooth solution. The VDO-FDEs are represented as a series of fractional Shifted Legendre Polynomials (SLPs). The residuals of these equations are evaluated at the SL-GL quadrature points, which yields a system of algebraic equations to be solved. In addition, we employ Fractional Shifted Legendre Gauss-Lobatto (FSL-GL) and Shifted Chebyshev Gauss-Radau (SC-GR) points to approximate solutions for time-nonlinear VDO-FDEs under given conditions. The time nonlinear VDO-FDEs is represented as a truncated series of Shifted Legendre Polynomials (SLPs) and Shifted Chebyshev Polynomials (SCP). The residuals of these equations at the FSL-GL and SC-GR quadrature points are estimated, leading to a system of algebraic equations that is subsequently solved. Numerical approaches are conducted to validate the effectiveness of this methodology.

The main contributions of this study can be summarized as follows:

1. We develop a novel and efficient spectral collocation framework for solving nonlinear VDO-FDEs with non-smooth and time-nonlinear solutions, a class of problems that has received very limited attention in the literature.

2. The proposed approach utilizes FSL-GL and SC-GR points to systematically approximate the solutions, transforming the VDO-FDEs into solvable algebraic systems while accurately capturing the non-local and hereditary properties of fractional derivatives.

3. A unified representation of nonlinear VDO-FDEs is constructed using truncated expansions in shifted Legendre and shifted Chebyshev polynomials, enabling the method to handle both variable-distributed order and time-dependent dynamics within the same computational framework.

4. The effectiveness of the proposed methodology is validated through comprehensive numerical experiments, demonstrating its robustness, accuracy, and exponential convergence in the presence of non-smooth solutions, outperforming conventional approaches.

5. This work establishes a flexible and generalizable framework for addressing a wide range of fractional models, underscoring the novelty and practical impact of combining advanced spectral collocation techniques with variable-distributed order fractional calculus.

This paper is structured as follows: Section 2 introduces the fundamental concepts. Section 3 addresses VDO-FDEs with non-smooth solutions, while section 4 focuses on time-nonlinear VDO-FDEs. Section 5 presents numerical examples, and section 6 concludes the study.

2. Fundamental concepts
2.1 Fractional calculus

This section specifies the fundamental terms utilized throughout the subsequent section, specifically the Left and Right Caputo formulas.

Definition 1 [34] Left and Right Caputo derivative $D^{\eta(\mathscr{Y})}$ of order $\eta(\mathscr{Y})$

$$^{C}D_{+}^{\eta(\mathscr{Y})}\hat{\mathscr{U}}(\mathscr{Y}) = \frac{1}{\Gamma(\gamma - \eta(\mathscr{Y}))}\left(\int_{0}^{\mathscr{Y}}(\mathscr{Y} - \kappa)^{\gamma - \eta(\mathscr{Y}) - 1}\hat{\mathscr{U}}^{(\gamma)}(\kappa)d\kappa\right), \quad \gamma - 1 < \eta(\mathscr{Y}) \le \gamma, \ \mathscr{Y} > 0. \tag{1}$$

$$^{C}D_{-}^{\eta(\mathscr{Y})}\hat{\mathscr{U}}(\mathscr{Y}) = \frac{(-1)^{\gamma}}{\Gamma(\rho - \eta(\mathscr{Y}))}\left(\int_{\mathscr{Y}}^{L}(\kappa - \mathscr{Y})^{\gamma - \eta(\mathscr{Y}) - 1}\hat{\mathscr{U}}^{(\gamma)}(\kappa)d\kappa\right), \quad \gamma - 1 < \eta(\mathscr{Y}) \le \gamma, \ \mathscr{Y} > 0. \tag{2}$$

Definition 2 [35] The Caputo Variable Order-Fractional (VO-F) derivative of order $\eta(\chi)$ is defined as

$$^{C}D_{\chi}^{\eta(\chi)}\hat{\mathscr{U}}(\mathscr{Y}, \chi) = \frac{1}{\Gamma(\gamma - \eta(\chi))}\int_{0}^{\chi}(\chi - \varepsilon)^{\gamma - \eta(\chi)}\frac{\partial\hat{\mathscr{U}}^{\gamma}(\mathscr{Y}, \varepsilon)}{\partial\varepsilon^{\gamma}}, \ d\varepsilon, \ \gamma - 1 < \eta(\chi) < \gamma, \ \mathscr{Y} > 0. \tag{3}$$

Definition 3 [35] The Riemann-Liouville VO-F derivative of order $\eta(\chi)$ is defined by

$$^{RL}D_{\chi}^{\eta(\chi)}\hat{\mathscr{U}}(\mathscr{Y}, \chi) = \frac{1}{\Gamma(\gamma - \eta(\chi))}\frac{d^{\gamma}}{dt^{\gamma}}\int_{0}^{\chi}(\chi - \varepsilon)^{\gamma - \eta(\chi) - 1}\hat{\mathscr{U}}(\mathscr{Y}, \varepsilon)d\varepsilon, \ \gamma - 1 < \eta(\chi) < \gamma, \ \mathscr{Y} > 0. \tag{4}$$

2.2 SLPs

The Legendre polynomials $\ell_{j}(\mathscr{Y})(j = 0, 1, \ldots)$ adheres to Rodrigues' formula [36].

$$\ell_j(\mathscr{Y}) = \frac{(-1)^j}{2^j j!} D^j \left((1 - \mathscr{Y}^2)^j \right) \tag{5}$$

Accordingly, $\ell_j^{(m)}(\mathscr{Y})$ is given by

$$\ell_j(\mathscr{Y}) = \frac{(-1)^j}{2^j j!} D^j \left((1 - \mathscr{Y}^2)^j \right) \tag{6}$$

where

$$C_m(j, \iota) = \frac{2^{m-1}(2\iota+1)\Gamma\left(\frac{m+j-\iota}{2}\right)\Gamma\left(\frac{m+j+\iota+1}{2}\right)}{\Gamma(m)\Gamma\left(\frac{2-m+j-\iota}{2}\right)\Gamma\left(\frac{3-m+j+\iota}{2}\right)}.$$

Then, we denote (u, v) and $\|u\|$ as the inner product and norm within the space $L^2[-1, 1]$. Complete orthogonal system is the set of $\ell_k(t)$ in $L^2[-1, 1]$

$$(\ell_j(t), \ell_k(\mathscr{Y})) = \int_{-1}^{1} \ell_j(\mathscr{Y})\ell_k(\mathscr{Y}) \, dt = h_k \delta_{jk}, \tag{7}$$

where $h_\iota = \dfrac{2}{2\iota+1}$ and δ_{jk} represents the Dirac delta function. Therefore for any $v \in L^2[-1, 1]$,

$$v(\mathscr{Y}) = \sum_{\iota=0}^{\infty} a_\iota \ell_\iota(\mathscr{Y}), \quad a_\iota = \frac{1}{h_\iota} \int_{-1}^{1} v(\mathscr{Y})\ell_\iota(\mathscr{Y}) \, d\mathscr{Y}. \tag{8}$$

The SLPs, denoted as $\ell_{L, \iota}(\mathscr{Y})$, are defined over the range $[0, L]$ and can be generated using the subsequent recursive formulan [36]:

$$(j+1)\ell_{L, \iota+1}(\mathscr{Y}) = (2j+1)\left(\frac{2\mathscr{Y}}{L} - 1\right)\ell_{L, \iota}(\mathscr{Y}) - j\ell_{L, \iota-1}(\mathscr{Y}), \qquad \iota = 1, 2, \cdots. \tag{9}$$

The analytical expression for $\ell_{L, \iota}(\mathscr{Y})$ can be expressed as

$$\ell_{L, \iota}(\mathscr{Y}) = \sum_{j=0}^{\iota} (-1)^{\iota+j} \frac{(\iota+j)!}{(\iota-j)! \, (j!)^2 \, L^j} \mathscr{Y}^j. \tag{10}$$

The condition for orthogonality is

$$\int_0^L \ell_{L,\iota}(t)\ell_{L,\iota}(\mathscr{Y})w_L(\mathscr{Y})\,d\mathscr{Y} = h_\iota^L\,\delta_{\iota j}, \tag{11}$$

where $w_L(\mathscr{Y}) = 1$ and $h_j^L = \dfrac{L}{2j+1}$.

If function $\hat{\mathscr{U}}(\mathscr{Y}) \in L^2[0,L]$. Next, it can be represented using $\ell_{L,\iota}(\mathscr{Y})$ as

$$\hat{\mathscr{U}}(\mathscr{Y}) = \sum_{\iota=0}^{\infty} c_\iota \ell_{L,\iota}(\mathscr{Y}).$$

The value of c_ι is determined by

$$c_\iota = \frac{1}{h_\iota^L}\int_0^L \hat{\mathscr{U}}(\mathscr{Y})\ell_{L,\iota}(\mathscr{Y})d\mathscr{Y}, \quad \iota = 0,\,1,\,2,\,\cdots. \tag{12}$$

Approximation $\hat{\mathscr{U}}(\mathscr{Y})$ can be expressed as:

$$\hat{\mathscr{U}}_N(\mathscr{Y}) \simeq \sum_{\iota=0}^{N} c_\iota \ell_{L,\iota}(\mathscr{Y}). \tag{13}$$

2.3 *SCP*

According to [36], Chebyshev polynomials are defined on the interval $[-1,\,1]$

$$\mathscr{C}_{\mathscr{J}}(\mathscr{Y}) = \cos(\mathscr{J}\arccos(\mathscr{Y})), \quad \mathscr{J} \geq 0. \tag{14}$$

Also

$$\mathscr{C}_{\mathscr{J}}(\pm 1) = (\pm 1)^{\mathscr{J}}, \quad \mathscr{C}_{\mathscr{J}}(-\mathscr{Y}) = (-1)^{\mathscr{J}}\mathscr{C}_{\mathscr{J}}(\mathscr{Y}). \tag{15}$$

Assume $w^c(t) = \dfrac{1}{\sqrt{1-\mathscr{Y}^2}}$, we present the subsequent $\|\hat{\mathscr{U}}\|$ and $(\hat{\mathscr{U}},\,\hat{\mathscr{V}})$ for the weighted space as

$$\|\hat{\mathscr{U}}\|_{w^c} = (\hat{\mathscr{U}},\,\hat{\mathscr{U}})_{w^c}^{\frac{1}{2}}, \qquad (\hat{\mathscr{U}},\,\hat{\mathscr{V}})_{w^c} = \int_{-1}^{1}\hat{\mathscr{U}}(\mathscr{Y})\,\hat{\mathscr{V}}(\mathscr{Y})w^c(\mathscr{Y})d\mathscr{Y}. \tag{16}$$

Chebyshev polynomials satisfy the following [36]:

$$\|\mathscr{C}_k\|_{w^c}^2 = h_k^c = \begin{cases} \dfrac{\varsigma_k}{2}\pi, & k = \mathscr{J}, \\ 0, & k \neq \mathscr{J}, \end{cases} \qquad \varsigma_0 = 2, \qquad \varsigma_k = 1, \qquad k \geq 1. \tag{17}$$

where norm and discrete inner product as

$$\|\hat{\mathscr{U}}\|_{w^c} = (\hat{\mathscr{U}}, \hat{\mathscr{U}})_{w^c}^{\frac{1}{2}}, \qquad (\hat{\mathscr{U}}, \hat{\mathscr{V}})_{w^c} = \sum_{\mathscr{J}=0}^{N} \hat{\mathscr{U}}(\mathscr{Y}_{N,\mathscr{J}}) \, \hat{\mathscr{V}}(\mathscr{Y}_{N,\mathscr{J}}) \, \varpi_{N,\mathscr{J}}^c. \tag{18}$$

The quadrature weights for the shifted rule $\varpi_{N,\mathscr{J}}^c$ are obtained by

$$\varpi_{N,j}^c = \frac{L}{2} \, \omega_j. \tag{19}$$

In particular, for the Chebyshev-Gauss-Lobatto case the weights ω_j on $[-1,\, 1]$ are

$$\omega_j = \begin{cases} \dfrac{\pi}{2N}, & j = 0,\, N, \\ \dfrac{\pi}{N}, & j = 1,\, \ldots,\, N-1, \end{cases}$$

$\mathscr{C}_{L,\,\alpha_1}(\mathscr{Y})$ represents the SCP specified on $[0,\, L]$. We obtain the analytic form of $\mathscr{C}_{L,\,\alpha_1}(\mathscr{Y})$ from,

$$\mathscr{C}_{L,\,\alpha_1}(\mathscr{Y}) = n \sum_{\mathscr{J}=0}^{\alpha_1} (-1)^{m-\mathscr{J}} \frac{(m+\mathscr{J}-1)! \, 2^{2\mathscr{J}}}{(\alpha_1 - \mathscr{J})! \, (2\mathscr{J})! \, T^{\mathscr{J}}} \, \mathscr{Y}^{\mathscr{J}}, \tag{20}$$

where $\mathscr{C}_{L,\,\alpha_1}(0) = (-1)^{\alpha_1}$ and $\mathscr{C}_{L,\,\alpha_1}(\mathscr{Y}) = 1$.

The condition for orthogonality is

$$\int_0^L \mathscr{C}_{L,\,\alpha_1}(\mathscr{Y}) \mathscr{C}_{L,\,\mathscr{J}}(\mathscr{Y}) W_L(\mathscr{Y}) d\mathscr{Y} = \delta_{\alpha_1 \mathscr{J}} \, h_{\mathscr{J}}^L, \tag{21}$$

where $w_T(\mathscr{Y}) = \dfrac{1}{\sqrt{T\mathscr{Y} - \mathscr{Y}^2}}$ and, $h_{\mathscr{J}}^T = \dfrac{c_{\mathscr{J}}}{2}\pi$, with $c_0 = 2$, $c_{\mathscr{J}} = 1$.

Similar to the preceding subsection, if $\hat{\mathscr{U}}(\mathscr{Y}) \in L^2_{w_L(\mathscr{Y})}[0,\, L]$. Then it can be expressed as $\mathscr{C}_{L,\,\mathscr{Y}}(\mathscr{Y})$ as

$$\hat{\mathscr{U}}(\mathscr{Y}) = \sum_{\mathscr{J}=0}^{\infty} a_{\mathscr{J}} \mathscr{C}_{L,\,\mathscr{J}}(\mathscr{Y}), \tag{22}$$

where

$$a_{\mathscr{J}} = \frac{1}{ch^T_{\mathscr{J}}} \int_0^L \hat{\mathscr{U}}(\mathscr{Y})\mathscr{C}_{L,\mathscr{J}}(\mathscr{Y})W_L(\mathscr{Y})d\mathscr{Y}, \ \mathscr{J} = 0, 1, 2, \cdots. \tag{23}$$

2.4 *Fractional-order shifted Legendre function*

Definition 4 Currently, let us define the new Fractional-Order Shifted Legendre Function (FO-SLP) as follows:

$$\ell^{(\lambda)}_{\mathscr{M},\mathscr{J}}(\chi) = \ell_{\mathscr{J}}\left(2\left(\frac{\chi}{\mathscr{M}}\right)^{\lambda} - 1\right) = 0 < \lambda < 1 \ \mathscr{J} = 0, 1, \cdots 0 \le \chi \le \mathscr{M}. \tag{24}$$

Theorem 1 For $\mathscr{W}^{(\lambda)}_{\mathscr{M},f}(\chi) = \lambda(\mathscr{M}^{\lambda} - \chi^{\lambda})\chi^{\lambda-1}$, the collection of FO-SLP forms a comprehensive $L^2_{\mathscr{W}^{(\lambda)}_f}[0, \mathscr{M}]$-orthogonal system

$$\int_0^{\mathscr{M}} \ell^{(\lambda)}_{\mathscr{M},i}(\chi) \ \ell^{(\lambda)}_{\mathscr{M},\mathscr{J}}(\chi) \ \mathscr{W}^{(\lambda)}_{\mathscr{M},f}(\chi) \ dx = \delta_{i\mathscr{J}} h^{(\lambda)}_{\mathscr{M},k}, \tag{25}$$

where $h^{(\lambda)}_{\mathscr{M},k} = \left(\frac{\mathscr{M}^{\lambda}}{2}\right) h_i$.

Proof. By the orthogonality property of Legendre polynomials, it follows that:

$$\int_{-1}^{1} \ell_i(\chi) \ \ell_{\mathscr{J}}(\chi) \ \mathscr{W}_f(\chi) \ d\chi = \delta_{i\mathscr{J}} h_i, \tag{26}$$

Given $\chi = 2\left(\frac{\chi}{\mathscr{M}}\right)^{\lambda} - 1$, we get

$$\int_{-1}^{1} \ell_i(\chi) \ \ell_{\mathscr{J}}(\chi) \ \mathscr{W}_f(\chi) \ d\chi = \frac{2\lambda}{\mathscr{M}^{\lambda}} \int_0^{\mathscr{M}} \chi^{\lambda-1} \ell_i\left(2\left(\frac{\chi}{\mathscr{M}}\right)^{\lambda} - 1\right) \ell_{\mathscr{J}}\left(2\left(\frac{\chi}{\mathscr{M}}\right)^{\lambda} - 1\right) \mathscr{W}_f\left(2\left(\frac{\chi}{\mathscr{M}}\right)^{\lambda} - 1\right) d\chi$$

$$= \left(\frac{2}{\mathscr{M}^{\lambda}}\right) \int_0^{\mathscr{M}} \ell^{(\lambda)}_{\mathscr{M},i}(\chi) \ \ell^{(\lambda)}_{\mathscr{M},\mathscr{J}}(\chi) \ \mathscr{W}^{(\lambda)}_{\mathscr{M},f}(\chi)d\chi \tag{27}$$

$$= \delta_{i\mathscr{J}} h_i.$$

Thus, we conclude

$$\int_0^{\mathscr{M}} \ell^{(\lambda)}_{\mathscr{M},i}(\chi)\, \ell^{(\lambda)}_{\mathscr{M},\mathscr{J}}(\chi)\, \mathscr{W}^{(\lambda)}_{\mathscr{M},f}(\chi)\, d\chi = \delta_{i\mathscr{J}}\left(\frac{\mathscr{M}}{2}\right)^{\lambda} h_i$$

$$\tag{28}$$

$$= \delta_{i\mathscr{J}} h^{(\lambda)}_{\mathscr{M},k}. \qquad \square$$

Corollary 1 Let $\mathscr{F}_N = span\{\ell^{(\lambda)}_{\mathscr{M},i} : 0 \le i \le N\}$ denote the finite-dimensional fractional-polynomial space. The function $\zeta(\chi) \in L^2_{\mathscr{W}^{(\lambda)}_f}[0, \mathscr{M}]$ can be expressed as

$$\zeta(\chi) = \sum_{i=0}^{\infty} \gamma_i \ell^{(\lambda)}_{\mathscr{M},i}(\chi), \quad \gamma_i = \frac{1}{h^{(\lambda)}_{\mathscr{M},k}} \int_0^{\mathscr{M}} \ell^{(\lambda)}_{\mathscr{M},i}(\chi)\, \zeta(\chi)\, \mathscr{W}^{(\lambda)}_{\mathscr{M},f}(\chi)\, d\chi.$$

Theorem 2 Caputo's fractional derivative with order δ, of FO-SLP $D^\delta_\chi \ell^{(\lambda)}_{\mathscr{M},\mathscr{J}}(\chi)$ can obtained in terms of FO-SLP as

$$D^\delta_\chi \ell^{(\lambda)}_{\mathscr{M},\mathscr{J}}(\chi) = \sum_{n=0}^{\mathscr{N}} \varepsilon^{(n,\,\mathscr{J},\,\lambda)}_\delta \ell^{(\lambda)}_{\mathscr{M},n}(\chi),$$

$$\tag{29}$$

where

$$\varepsilon^{(n,\,\mathscr{J},\,\lambda)}_\delta = \sum_{k=1}^{\mathscr{J}} \sum_{s=0}^{n} \frac{E^{(\lambda,\,\mathscr{J})}_k E^{(\lambda,\,n)}_s}{h^{(\lambda)}_{\mathscr{M},n}} \frac{k\lambda\Gamma(k\lambda)\Gamma\left(k+s-\dfrac{\delta}{\lambda}+1\right)T^{\lambda(k+s+1)-\delta}}{\Gamma(k\lambda-\delta+1)\Gamma\left(k+s-\dfrac{\delta}{\lambda}+2\right)}.$$

Proof. The analytical form of $\ell^{(\lambda)}_{\mathscr{M},\mathscr{J}}(\chi)$ is expressed as

$$\ell^{(\lambda)}_{\mathscr{M},\mathscr{J}}(\chi) = \sum_{k=0}^{\mathscr{J}} E^{(\lambda,\,\mathscr{J})}_k \chi^{\lambda k},$$

where

$$E^{(\lambda,\,\mathscr{J})}_k = \frac{(-1)^{\mathscr{J}-k}(\Gamma(\mathscr{J}+1)\Gamma(\mathscr{J}+k+1))}{k!(\mathscr{J}-k)!\Gamma(k+1)\Gamma(\mathscr{J}+1)\mathscr{M}^{\lambda k}}.$$

Using the definition of the Caputo derivative, we obtain:

$$D^\delta_\chi(\chi^{\lambda k}) = \frac{k\lambda\Gamma(k\lambda)\chi^{k\lambda-\delta}}{\Gamma(k\lambda-\delta+1)},$$

thus

$$D_\chi^\delta(\ell_{\mathscr{M},\mathscr{J}}^{(\lambda)}(\chi)) = \ell_{\mathscr{M},\mathscr{J}}^{(\delta,\lambda)}(\chi)$$

$$= \sum_{k=1}^{\mathscr{J}} E_k^{(\lambda,\mathscr{J})} \frac{k\lambda\Gamma(k\lambda)\chi^{k\lambda-\delta}}{\Gamma(k\lambda-\delta+1)}.$$

Using Corollary 1, we may define

$$\chi^{k\lambda-\delta} = \sum_{n=0}^{\mathscr{N}} b_{k,n} \ell_{\mathscr{M},n}^{(\lambda)}(\chi), \tag{30}$$

where

$$b_{k,n} = \frac{1}{h_{\mathscr{M},n}^{(\lambda)}} \sum_{s=0}^{n} \frac{\Gamma\left(k+s-\dfrac{\delta}{\lambda}+1\right) T^{\lambda(k+s+1)-\delta}}{\Gamma\left(k+s-\dfrac{\delta}{\lambda}+2\right)} E_s^{(\lambda,n)}.$$

Thence, we conclude

$$D_\chi^\delta(\ell_{\mathscr{M},\mathscr{J}}^{(\lambda)}(\chi)) = \sum_{n=0}^{\mathscr{N}} \varepsilon_\delta^{(n,\mathscr{J},\lambda)} \ell_{\mathscr{M},n}^{(\lambda)}(\chi), \tag{31}$$

where

$$\varepsilon_\delta^{(n,\mathscr{J},\lambda)} = \sum_{k=1}^{\mathscr{J}} E_k^{(\lambda,\mathscr{J})} \frac{k\lambda\Gamma(k\lambda)}{\Gamma(k\lambda-\delta+1)} b_{k,n}. \qquad \square$$

3. Spectral collocation for solving non-linear VDO-FDEs

This section presents a computational approach that extends the capabilities of the Shifted Legendre-Gauss-Lobatto Collocation (SL-GL-C) scheme for solving nonlinear VDO-FDEs. Collocation points are strategically chosen at the interpolation nodes of the SL-GL method. The core of the proposed algorithm involves discretizing the nonlinear VDO-FDEs, which leads to a system of algebraic equations for determining the unknown coefficients.

Specifically, we focus on the subsequent non-linear VDO-FDEs.

$$^cD_{\mathscr{Y}}^{W_1(\eta(\mathscr{Y}))} \hat{\mathscr{U}}(\mathscr{Y}) = G(\mathscr{Y}, \hat{\mathscr{U}}(\mathscr{Y})), \tag{32}$$

with initial condition

$$\hat{\mathscr{U}}(0) = 0, \tag{33}$$

where

$$D_{\mathscr{Y}}^{W_1(\eta(\mathscr{Y}))}\hat{\mathscr{U}}(\mathscr{Y}) = \int_0^1 W_1(\eta(\mathscr{Y}))D^{\eta(\mathscr{Y})}\hat{\mathscr{U}}(\mathscr{Y})d\eta(\mathscr{Y}), \tag{34}$$

the functions $\hat{\mathscr{U}}(\mathscr{Y})$ is an unknown function and $D^{\eta(\mathscr{Y})}\hat{\mathscr{U}}(\mathscr{Y})$ represent the fractional Caputo derivative of order $\eta(\mathscr{Y})$, and the function $G(\mathscr{Y}, \hat{\mathscr{U}}(\mathscr{Y}))$ denotes the nonlinear source term.

Definition 5 The fractional Caputo VO-F derivative [22] of order $\eta(\mathscr{Y})$ can be described as follows:

$$D^{\eta(\mathscr{Y})}\hat{\mathscr{U}}(\mathscr{Y}) = \frac{1}{\Gamma(\gamma - \eta(\mathscr{Y}))} \int_0^{\mathscr{Y}} (\mathscr{Y} - \varepsilon)^{\gamma - \eta(\mathscr{Y}) - 1}\hat{\mathscr{U}}^{(\gamma)}(\varepsilon)d\varepsilon, \quad \gamma - 1 < \eta(\mathscr{Y}) \le \gamma, \ \mathscr{Y} > 0, \tag{35}$$

here, γ represents the ceiling function applied to $\eta(\mathscr{Y})$.

If $\hat{\mathscr{U}}_{\text{Approx}}(\mathscr{Y})$ is defined as an approximation of (32):

$$\hat{\mathscr{U}}_{\text{Approx}}(\mathscr{Y}) = \sum_{\tau_1 = 0, 1, \ldots, v_2} a_{\tau_1}\mathscr{L}_{L, \tau_1}(\mathscr{Y}), \tag{36}$$

where $\mathscr{L}_{L, \tau_1}(\mathscr{Y})$ is SLPs, and the derivative $D^{\eta(\mathscr{Y})}$ of $\hat{\mathscr{U}}_{\text{Approx}}(\mathscr{Y})$ is:

$$D^{\eta(\mathscr{Y})}\hat{\mathscr{U}}_{\text{Approx}}(\mathscr{Y}) = \sum_{\tau_1 = 0, 1, \ldots, v_2} a_{\tau_1}D^{\eta(\mathscr{Y})}\big(\mathscr{L}_{L, \tau_1}(\mathscr{Y})\big). \tag{37}$$

By using the Caputo derivative of $\eta(\mathscr{Y})$ as defined in Definition (35), we obtain:

$$D^{\eta(\mathscr{Y})}\mathscr{Y}^{\tau_1} = \frac{1}{\Gamma(1 - \eta(\mathscr{Y}))} \int_0^{\mathscr{Y}} \frac{\vartheta^{(\tau_1)}}{(\mathscr{Y} - \vartheta)^{\eta(\mathscr{Y})}}d\vartheta$$

$$= \frac{\mathscr{Y}^{\tau_1 - \eta(\mathscr{Y})}\Gamma(1 + \tau_1)}{\Gamma(1 + \tau_1 - \eta(\mathscr{Y}))}. \tag{38}$$

Therefore, it follows that:

$$D^{\eta(\mathscr{Y})}\mathscr{L}_{L,\,\tau_1}(\mathscr{Y}) = \sum_{\tau_1=0,\,1,\,...,\,\nu_2}(-1)^{\tau_1-\nu_2}\frac{(\nu_2+\tau_1-1)!\,2^{2\tau_1}}{(\nu_2-\tau_1)!\,(2\tau_1)!\,L^{\tau_1}}\,D^{\eta(\mathscr{Y})}\mathscr{Y}^{\tau_1}$$

$$= \sum_{\tau_1=0,\,1,\,...,\,\nu_2}(-1)^{\tau_1-\nu_2}\frac{\tau_1!(\nu_2+\tau_1-1)!\,2^{2\tau_1}}{(\nu_2-\tau_1)!\,(2\tau_1)!\,L^{\tau_1}(\tau_1-\eta(\mathscr{Y}))!}\,\mathscr{Y}^{\tau_1-\eta(\mathscr{Y})}. \tag{39}$$

Then, we get the following:

$$D^{\eta(\mathscr{Y})}\hat{\mathscr{U}}_{\text{Approx}}(\mathscr{Y}) = \sum_{\tau_1=0,\,1,\,...,\,\nu_2}a_{\tau_1}D^{\eta(\mathscr{Y})}\big(\mathscr{L}_{L,\,\tau_1}(\mathscr{Y})\big) = \sum_{\tau_1=0,\,1,\,...,\,\nu_2}a_{\tau_1}\Delta_{L,\,\tau_1}(\mathscr{Y}). \tag{40}$$

Moreover

$$\int_0^1 W_1(\eta(\mathscr{Y}))D_{\mathscr{Y}}^{\eta(\mathscr{Y})}\hat{\mathscr{U}}(\mathscr{Y})d\eta(\mathscr{Y}) = \int_0^1 W_1(\eta(\mathscr{Y}))\sum_{\tau_1=0,\,1,\,...,\,\nu_2}a_{\tau_1}\Delta_{L,\,\tau_1}(\mathscr{Y})d\eta(\mathscr{Y})$$

$$= \sum_{\tau_1=0,\,1,\,...,\,\nu_2}a_{\tau_1}\left(\int_0^1 W_1(\eta(\mathscr{Y}))\Delta_{L,\,\tau_1}(\eta(\mathscr{Y}),\,\mathscr{Y})d\eta(\mathscr{Y})\right)$$

$$= \sum_{\tau_1=0,\,1,\,...,\,\nu_2}\sum_{i=0}^{\nu_2}a_{\tau_1}\varpi_{\nu_2,\,i}W_1(\eta(\mathscr{Y})_{\nu_2,\,i})\Delta_{L,\,\tau_1}(\eta(\mathscr{Y})_{\nu_2,\,i},\,\mathscr{Y})$$

$$= \sum_{\tau_1=0,\,1,\,...,\,\nu_2}a_{\tau_1}\zeta_{L,\,\tau_1}(\mathscr{Y}). \tag{41}$$

Equation (32) can be rewritten as:

$$\sum_{\tau_1=0,\,1,\,...,\,\nu_2}a_{\tau_1}\zeta_{L,\,\tau_1}(\mathscr{Y}) = G\left(\mathscr{Y},\,\sum_{\tau_1=0,\,1,\,...,\,\nu_2}a_{\tau_1}\mathscr{L}_{L,\,\tau_1}(\mathscr{Y})\right). \tag{42}$$

The residual of Eq. (42) is set to zero by utilizing the SL-GL collocation technique at ν_2-1, of the SL-GL points. By utilizing Eq. (36)-(42), then (32) can be written as:

$$\sum_{\tau_1=0,\,1,\,...,\,\nu_2}a_{\tau_1}\zeta_{L,\,\tau_1}(\mathscr{Y}_{L,\,\nu_2,\,i}) = G\left(\mathscr{Y}_{L,\,\nu_2,\,i},\,\sum_{\tau_1=0,\,1,\,...,\,\nu_2}a_{\tau_1}\mathscr{L}_{L,\,\tau_1}(\mathscr{Y}_{L,\,\nu_2,\,i})\right),\,i=1,\,...,\,\nu_2. \tag{43}$$

Using Eq. (33) and (36), we acquire:

$$\sum_{\tau_1=0,\,1,\,...,\,\nu_2} a_{\tau_1}\mathscr{L}_{L,\,\tau_1}(0) = 0. \tag{44}$$

Equations (43) and (44) form a set of (ν_2+1) algebraic equations involving the variables $a_{\tau_1}\ \tau_1 = 0,\,1,\,...,\,\nu_2$.

$$\begin{cases} \displaystyle\sum_{\tau_1=0,\,1,\,...,\,\nu_2} (-1)^{\tau_1} a_{\tau_1} = d_0, \\[2mm] \displaystyle\sum_{\tau_1=0,\,1,\,...,\,\nu_2} a_{\tau_1}\zeta_{L,\,\tau_1}(\mathscr{Y}_{L,\,\nu_2,\,i}) = G\left(\mathscr{Y}_{L,\,\nu_2,\,i},\,\sum_{\tau_1=0,\,1,\,...,\,\nu_2} a_{\tau_1}\mathscr{L}_{L,\,\tau_1}(\mathscr{Y}_{L,\,\nu_2,\,i})\right)\ i = 1,\,\ldots,\,\nu_2. \end{cases} \tag{45}$$

Finally, solving the system is straightforward, allowing $\hat{\mathscr{U}}_{\text{Approx}}$ to be expressed in a closed form.

4. Time nonlinear VDO-FDEs

We present a numerical methodology that extends the solution capabilities of time-nonlinear VDO-FDEs using the Fractional Shifted Legendre Gauss-Lobatto Collocation (FSL-GL-C) and Shifted Chebyshev Gauss-Radau Collocation (SC-GR-C) schemes. Collocation points for the spatial and temporal variables are selected at the FSL-GL and SC-GR interpolation nodes, respectively. The core of the proposed algorithm involves discretizing the time-nonlinear VDO-FDEs, resulting in a system of algebraic equations for determining the unknown coefficients.

Specifically, we focus on the subsequent time nonlinear VDO-FDEs.

$$D_\chi^{\omega(\eta(\chi))}\hat{\mathscr{U}}(\mathscr{Y},\,\chi) + \frac{\partial^2\hat{\mathscr{U}}(\mathscr{Y},\,\chi)}{\partial\mathscr{Y}^2} = G(\mathscr{Y},\,\chi,\,\hat{\mathscr{U}}(\mathscr{Y},\,\chi)), \tag{46}$$

with the initial-boundary conditions

$$\hat{\mathscr{U}}(\mathscr{Y},\,0) = \eta_1(\mathscr{Y}),\qquad \hat{\mathscr{U}}(0,\,\chi) = \eta_2(\chi),\qquad \hat{\mathscr{U}}(L,\,\chi) = \eta_3(\chi), \tag{47}$$

where $D_\chi^{\omega(\eta(\chi))}\hat{\mathscr{U}}(\mathscr{Y},\,\chi) = \int_0^1 \aleph(\omega(\eta(\chi)))\,^cD_\chi^{\omega(\eta(\mathscr{Y}))}\check{\phi}(\mathscr{Y},\,\chi)\,d\eta(\chi)$, and $\hat{\mathscr{U}}(\mathscr{Y},\,\chi)$ is unknown function, while $\nu(\mathscr{Y},\,\chi),\eta_1(\mathscr{Y}),\eta_2(\chi),\eta_3(\chi)$ are given functions.

The approximate solution is chosen as

$$\hat{\mathscr{U}}_{\mathscr{N},\,\mathscr{M}}(\mathscr{Y},\,\chi) = \sum_{\substack{\hat{s}=0,\,1,\,...,\,\mathscr{N} \\ \hat{t}=0,\,1,\,...,\,\mathscr{M}}} \tilde{e}_{\hat{s},\,\hat{t}}\mathscr{C}_{L,\,\hat{s}}(\mathscr{Y})\ell_{T,\,\hat{t}}^{(\lambda)}(\chi), \tag{48}$$

where $\ell_{T,\,\hat{t}}^{(\lambda)}(\chi)$ is fractional shifted Legendre polynomials, and $\mathscr{C}_{L,\,\hat{s}}(\mathscr{Y})$ is shifted Chebyshev polynomials. Next, we evaluate spatial partial derivatives $\dfrac{\partial\hat{\mathscr{U}}(\mathscr{Y},\,\chi)}{\partial\mathscr{Y}},\ \dfrac{\partial^2\hat{\mathscr{U}}(\mathscr{Y},\,\chi)}{\partial\mathscr{Y}^2}$ as

$$\frac{\partial \hat{\mathscr{U}}(\mathscr{Y},\chi)}{\partial \mathscr{Y}} = \sum_{\substack{\hat{s}=0,\,1,\,...,\,\mathscr{N} \\ \hat{t}=0,\,1,\,...,\,\mathscr{M}}} \tilde{e}_{\hat{s},\,\hat{t}} \frac{\partial \mathscr{C}_{L,\,\hat{s}}(\mathscr{Y})}{\partial \mathscr{Y}} \ell_{T,\,\hat{t}}(\chi) = \sum_{\substack{\hat{s}=0,\,1,\,...,\,\mathscr{N} \\ \hat{t}=0,\,1,\,...,\,\mathscr{M}}} \tilde{e}_{\hat{s},\,\hat{t}} \mathscr{C}_{L,\,\hat{s}}^{(1)}(\mathscr{Y}) \ell_{T,\,\hat{t}}^{(\lambda)}(\chi), \tag{49}$$

$$\frac{\partial^2 \hat{\mathscr{U}}(\mathscr{Y},\chi)}{\partial \mathscr{Y}^2} = \sum_{\substack{\hat{s}=0,\,1,\,...,\,\mathscr{N} \\ \hat{t}=0,\,1,\,...,\,\mathscr{M}}} \tilde{e}_{\hat{s},\,\hat{t}} \frac{\partial^2 \mathscr{C}_{L,\,\hat{s}}(\mathscr{Y})}{\partial \mathscr{Y}^2} \ell_{T,\,\hat{t}}(\chi) = \sum_{\substack{\hat{s}=0,\,1,\,...,\,\mathscr{N} \\ \hat{t}=0,\,1,\,...,\,\mathscr{M}}} \tilde{e}_{\hat{s},\,\hat{t}} \mathscr{C}_{L,\,\hat{s}}^{(2)}(\mathscr{Y}) \ell_{T,\,\hat{t}}^{(\lambda)}(\chi). \tag{50}$$

Additionally, ${}^c D_\chi^{\omega(\eta(\chi))} \hat{\mathscr{U}}(\mathscr{Y},\chi)$, Caputo's fractional derivative with order ω, has been given by

$$\begin{aligned}
{}^c D_\chi^{\omega(\eta(\chi))} \hat{\mathscr{U}}(\mathscr{Y},\chi) &= \sum_{\substack{\hat{s}=0,\,1,\,...,\,\mathscr{N} \\ \hat{t}=0,\,1,\,...,\,\mathscr{M}}} \tilde{e}_{\hat{s},\,\hat{\chi}} \mathscr{C}_{L,\,\hat{s}}(\mathscr{Y}) \, {}^c D_\chi^{\omega(\eta(\chi))}(\ell_{\hat{\chi}}^{(\lambda)}(\chi)) \\
&= \sum_{\substack{\hat{s}=0,\,1,\,...,\,\mathscr{N} \\ \hat{\chi}=0,\,1,\,...,\,\mathscr{M}}} \tilde{e}_{\hat{s},\,\hat{\chi}} \mathscr{C}_{L,\,\hat{s}}(\mathscr{Y}) \ell_{\hat{\chi},\,\omega}^{(\lambda)}(\chi).
\end{aligned} \tag{51}$$

The distributed fractional term is handled as follows by using FSL-GL quadrature:

$$\begin{aligned}
\int_0^1 \aleph(\omega(\eta(\chi))) \, {}^c D_\chi^{\omega(\eta(\mathscr{Y}))} \check{\phi}(\mathscr{Y},\chi) d\eta(\chi) &= \int_0^1 \aleph(\omega(\eta(\chi))) \sum_{\substack{\hat{s}=0,\,1,\,...,\,\mathscr{N} \\ \hat{\chi}=0,\,1,\,...,\,\mathscr{M}}} \tilde{e}_{\hat{s},\,\hat{\chi}} \mathscr{C}_{L,\,\hat{s}}(\mathscr{Y}) \hat{\mathscr{U}}_{\hat{\chi},\,\eta(\chi)}^{(\eta(\chi))} \\
&= \sum_{\substack{\hat{s}=0,\,1,\,...,\,\mathscr{N} \\ \hat{\chi}=0,\,1,\,...,\,\mathscr{M}}} \tilde{e}_{\hat{s},\,\hat{\chi}} \mathscr{C}_{L,\,\hat{s}}(\mathscr{Y}) \int_0^1 \aleph(\omega(\eta(\chi))) \ell_{\hat{\chi},\,\eta(\mathscr{Y})}^{(\eta(\chi))}(\chi) d\eta(\mathscr{Y}) \\
&= \sum_{\substack{\hat{s}=0,\,1,\,...,\,\mathscr{N} \\ \hat{\chi}=0,\,1,\,...,\,\mathscr{M}}} \tilde{e}_{\hat{s},\,\hat{\chi}} \mathscr{C}_{L,\,\hat{s}}(\mathscr{Y}) \, {}_0\mathscr{E}_{\hat{\chi}}^{(\eta(\chi))}(\chi),
\end{aligned} \tag{52}$$

where

$$\begin{aligned}
\mathscr{E}_{\hat{\chi}}^{(\eta(\chi))}(\chi) &= \int_0^1 \aleph(\omega(\eta(\chi))) \ell_{\hat{\chi},\,\eta(\chi)}^{(\eta(\chi))}(\chi) d\eta(\chi) \\
&= \sum_{\hat{w}=0,\,1,\,...,\,\mathscr{W}} {}_0\mathbf{W}_1^{\mathscr{W},\,\hat{w}} \aleph({}_0\Omega_1^{\hat{w}}) \ell_{\hat{\chi},\,{}_0\eta(\chi)}^{\eta(\chi)}(\chi).
\end{aligned} \tag{53}$$

Currently, using (48)-(51), we may rewrite (46) as:

$$\sum_{\substack{\hat{s}=0,\,1,\,\ldots,\,\mathcal{N} \\ \hat{\chi}=0,\,1,\,\ldots,\,\mathcal{M}}} \tilde{e}_{\hat{s},\,\hat{\chi}}\mathscr{C}_{L,\,\hat{s}}(\mathscr{Y})_0\mathscr{E}_{\hat{\chi}}^{(\eta(\chi))}(\chi) + \sum_{\substack{\hat{s}=0,\,1,\,\ldots,\,\mathcal{N} \\ \hat{t}=0,\,1,\,\ldots,\,\mathcal{M}}} \tilde{e}_{\hat{s},\,\hat{t}}\mathscr{C}_{L,\,\hat{s}}^{(2)}(\mathscr{Y})\ell_{T,\,\hat{t}}^{(\lambda)}(\chi))$$

$$= G\left(\mathscr{Y},\,\chi,\,\sum_{\substack{\hat{s}=0,\,1,\,\ldots,\,\mathcal{N} \\ \hat{t}=0,\,1,\,\ldots,\,\mathcal{M}}} \tilde{e}_{\hat{s},\,\hat{t}}\mathscr{C}_{L,\,\hat{s}}(\mathscr{Y})\ell_{T,\,\hat{t}}^{(\lambda)}(\chi)\right). \tag{54}$$

By treating the Dirichlet boundary and initial conditions as

$$\begin{cases} \hat{\mathscr{U}}(\mathscr{Y},\,0) = \displaystyle\sum_{\substack{\hat{s}=0,\,1,\,\ldots,\,\mathcal{N} \\ \hat{t}=0,\,1,\,\ldots,\,\mathcal{M}}} \tilde{e}_{\hat{s},\,\hat{t}}\mathscr{C}_{L,\,\hat{s}}(\mathscr{Y})\ell_{T,\,\hat{t}}^{(\lambda)}(0) = \eta_1(\mathscr{Y}), \\[2em] \hat{\mathscr{U}}(0,\,\chi) = \displaystyle\sum_{\substack{\hat{s}=0,\,1,\,\ldots,\,\mathcal{N} \\ \hat{t}=0,\,1,\,\ldots,\,\mathcal{M}}} \tilde{e}_{\hat{s},\,\hat{t}}\mathscr{C}_{L,\,\hat{s}}(0)\ell_{T,\,\hat{t}}^{(\lambda)}(\chi) = \eta_1(\chi), \\[2em] \hat{\mathscr{U}}(L,\,\chi) = \displaystyle\sum_{\substack{\hat{s}=0,\,1,\,\ldots,\,\mathcal{N} \\ \hat{t}=0,\,1,\,\ldots,\,\mathcal{M}}} \tilde{e}_{\hat{s},\,\hat{t}}\mathscr{C}_{L,\,\hat{s}}(L)\ell_{T,\,\hat{t}}^{(\lambda)}(\chi) = \eta_1(\chi). \end{cases} \tag{55}$$

The residual of Eq. (54) is set to zero by utilizing the FSL-GL-C and SC-GR-C technique at $(M-1)(N-1)$. Then we write:

$$\sum_{\substack{\hat{s}=0,\,1,\,\ldots,\,\mathcal{N} \\ \hat{\chi}=0,\,1,\,\ldots,\,\mathcal{M}}} \tilde{e}_{\hat{s},\,\hat{\chi}}\mathscr{C}_{L,\,\hat{s}}(\mathscr{Y}_{L,\,s})_0\mathscr{E}_{\chi\hat{T},\,\tau}^{((\eta(\chi)))}(\chi_{T,\,\tau}) + \sum_{\substack{\hat{s}=0,\,1,\,\ldots,\,\mathcal{N} \\ \hat{t}=0,\,1,\,\ldots,\,\mathcal{M}}} \tilde{e}_{\hat{s},\,\hat{t}}\mathscr{C}_{L,\,\hat{s}}^{(2)}(\mathscr{Y}_{L,\,s})\ell_{T,\,\hat{t}}^{(\lambda)}(\chi_{T,\,\tau})$$

$$= G\left(\mathscr{Y}_{L,\,s},\,\chi_{T,\,\tau},\,\sum_{\substack{\hat{s}=0,\,1,\,\ldots,\,\mathcal{N} \\ \hat{t}=0,\,1,\,\ldots,\,\mathcal{M}}} \tilde{e}_{\hat{s},\,\hat{t}}\mathscr{C}_{L,\,\hat{s}}(\mathscr{Y}_{L,\,s})\ell_{T,\,\hat{t}}^{(\lambda)}(\chi_{T,\,\tau})\right), \tag{56}$$

we reliance on Eq. (55) we obtain

$$\begin{cases} \displaystyle\sum_{\substack{\hat{s}=0,\,1,\,\ldots,\,\mathcal{N} \\ \hat{t}=0,\,1,\,\ldots,\,\mathcal{M}}} \tilde{e}_{\hat{s},\,\hat{t}}\mathscr{C}_{L,\,\hat{s}}(\mathscr{Y}_{L,\,s})\ell_{T,\,\hat{t}}^{(\lambda)}(0) = \eta_1(\mathscr{Y}_{L,\,s}), \\[2em] \displaystyle\sum_{\substack{\hat{s}=0,\,1,\,\ldots,\,\mathcal{N} \\ \hat{t}=0,\,1,\,\ldots,\,\mathcal{M}}} \tilde{e}_{\hat{s},\,\hat{t}}\mathscr{C}_{L,\,\hat{s}}(0)\ell_{T,\,\hat{t}}^{(\lambda)}(\chi_{T,\,\tau}) = \eta_1(\chi_{T,\,\tau}), \\[2em] \displaystyle\sum_{\substack{\hat{s}=0,\,1,\,\ldots,\,\mathcal{N} \\ \hat{t}=0,\,1,\,\ldots,\,\mathcal{M}}} \tilde{e}_{\hat{s},\,\hat{t}}\mathscr{C}_{L,\,\hat{s}}(L)\ell_{T,\,\hat{t}}^{(\lambda)}(\chi_{T,\,\tau}) = \eta_1(\chi_{T,\,\tau}). \end{cases} \tag{57}$$

Combining Eq. (56) and (57) we obtain

$$\begin{cases} \displaystyle\sum_{\substack{\hat{s}=0,\,1,\,...,\,\mathscr{N} \\ \hat{\chi}=0,\,1,\,...,\,\mathscr{M}}} \tilde{e}_{\hat{s},\,\hat{\chi}}\mathscr{C}_{L,\,\hat{s}}(\mathscr{Y}_{L,\,s})\,_0\mathscr{E}_{\chi_{\hat{T},\,\tau}}^{(\eta(\chi))}(\chi_{T,\,\tau}) + \displaystyle\sum_{\substack{\hat{s}=0,\,1,\,...,\,\mathscr{N} \\ \hat{t}=0,\,1,\,...,\,\mathscr{M}}} \tilde{e}_{\hat{s},\,\hat{t}}\mathscr{C}_{L,\,\hat{s}}^{(2)}(\mathscr{Y}_{L,\,s})\ell_{T,\,\hat{t}}^{(\lambda)}(\chi_{T,\,\tau}) \\[2em] = \ G\left(\mathscr{Y}_{L,\,s},\,\chi_{T,\,\tau},\, \displaystyle\sum_{\substack{\hat{s}=0,\,1,\,...,\,\mathscr{N} \\ \hat{t}=0,\,1,\,...,\,\mathscr{M}}} \tilde{e}_{\hat{s},\,\hat{t}}\mathscr{C}_{L,\,\hat{s}}(\mathscr{Y}_{L,\,s})\ell_{T,\,\hat{t}}^{(\lambda)}(\chi_{T,\,\tau})\right), \\[2em] \displaystyle\sum_{\substack{\hat{s}=0,\,1,\,...,\,\mathscr{N} \\ \hat{t}=0,\,1,\,...,\,\mathscr{M}}} \tilde{e}_{\hat{s},\,\hat{t}}\mathscr{C}_{L,\,\hat{s}}(\mathscr{Y}_{L,\,s})\ell_{T,\,\hat{t}}^{(\lambda)}(0) = \eta_1(\mathscr{Y}_{L,\,s}), \\[1.5em] \displaystyle\sum_{\substack{\hat{s}=0,\,1,\,...,\,\mathscr{N} \\ \hat{t}=0,\,1,\,...,\,\mathscr{M}}} \tilde{e}_{\hat{s},\,\hat{t}}\mathscr{C}_{L,\,\hat{s}}(0)\ell_{T,\,\hat{t}}^{(\lambda)}(\chi_{T,\,\tau}) = \eta_1(\chi_{T,\,\tau}), \\[1.5em] \displaystyle\sum_{\substack{\hat{s}=0,\,1,\,...,\,\mathscr{N} \\ \hat{t}=0,\,1,\,...,\,\mathscr{M}}} \tilde{e}_{\hat{s},\,\hat{t}}\mathscr{C}_{L,\,\hat{s}}(L)\ell_{T,\,\hat{t}}^{(\lambda)}(\chi_{T,\,\tau}) = \eta_1(\chi_{T,\,\tau}). \end{cases} \tag{58}$$

This yields a system of algebraic equations that is straightforward to solve.

5. Numerical results

The efficacy and precision of the proposed approach are demonstrated through the examples, where the Absolute Error (AEs) refers to the disparity between the observed and predicted solution:

$$\text{AEs}(\mathscr{Y}) = |\mathscr{U}(\mathscr{Y}) - \hat{\mathscr{U}}(\mathscr{Y})|. \tag{59}$$

For the point $\mathscr{Y}$, the approximate and exact solutions are $\mathscr{R}(\mathscr{Y})$ and $\hat{\mathscr{U}}(\mathscr{Y})$. The approach for determining the largest AEs (L_∞) Maximum Absolute Error (MAE) and (L_2) is as described below:

$$L_\infty = \max\{\text{AEs}(\mathscr{Y})\}. \tag{60}$$

Example 1 Consider the non-linear VDO-FDEs with non-smooth solution:

$$\begin{cases} D_{\mathscr{Y}}^{W_1(\eta(\mathscr{Y}))}\hat{\mathscr{U}}(\mathscr{Y}) - \hat{\mathscr{U}}(\mathscr{Y}) + (\hat{\mathscr{U}}(\mathscr{Y}))^2 = G(\mathscr{Y}), \\ \mathscr{Y}(0) = 0. \end{cases} \tag{61}$$

$G(\mathscr{Y})$ is given from the exact solution $\hat{\mathscr{U}}(\mathscr{Y}) = \mathscr{Y}^{\frac{5}{2}}\sin(\mathscr{Y})$, where $D_{\mathscr{Y}}^{W_1(\eta(\mathscr{Y}))}\hat{\mathscr{U}}(\mathscr{Y}) = \int_0^1 \Gamma(\eta(\mathscr{Y}) - 0.5) D^{\eta(\mathscr{Y})}\hat{\mathscr{U}}(\mathscr{Y})d\eta(\mathscr{Y})$.

We obtain L_∞ with various values of v_2 in Table 1. The findings indicate that the proposed method offers higher levels of accuracy. Furthermore, it is noteworthy that satisfactory approximations can be achieved using a limited number of data points. Figure 1 represents the AEs of Example 1 when $v_1 = 16$, $\eta(\mathscr{Y}) = \mathscr{Y}^2\cos(x)$ and $\eta(\mathscr{Y}) = \dfrac{\mathscr{Y}^2}{3}$ respectively. Figure 2 compare the exact and approximate solutions. Figure 3 depicts the convergence decay curve of Example 1. The results show that, even by a few points, our technique is more accurate. Table 1 demonstrates that the proposed spectral

method achieves high accuracy even with a moderate number of collocation points. The MAE decreases exponentially as v_2 increases, indicating rapid convergence. Furthermore, both forms of $\eta(\mathscr{Y})$ yield comparable accuracy, highlighting the robustness of the approach. The results indicate that the proposed method accurately captures the non-smooth behavior of the solution. The convergence of $\hat{\mathscr{U}}_{\text{Approx}}(\mathscr{Y})$ towards the exact solution demonstrates that even a limited number of collocation points is sufficient to resolve the main features of the solution, including its rapid growth and oscillatory behavior. This suggests that the method can be efficiently applied to other nonlinear VDO-FDEs with similar complexities.

Table 1. The Maximum Absolute Error (MAE) of Example 1 for various values of v_2 and $\eta(\mathscr{Y})$

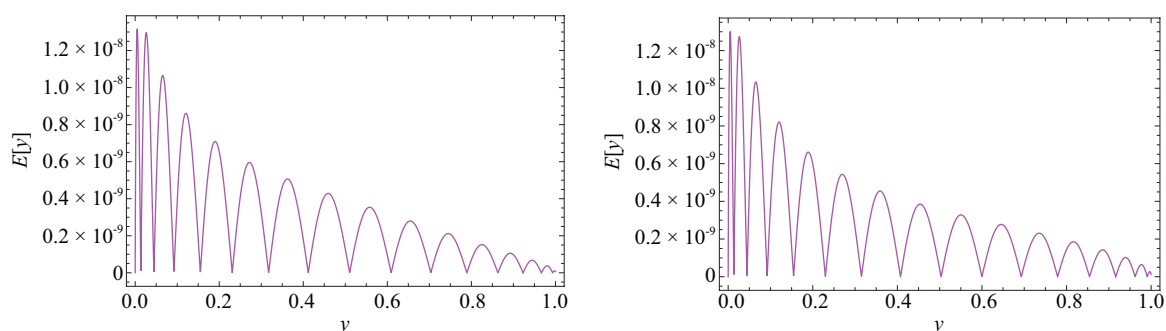| $\eta(\mathscr{Y})$	$v_2 = 4$	$v_2 = 6$	$v_2 = 8$	$v_2 = 10$	$v_2 = 12$	$v_2 = 14$	$v_2 = 16$	$v_2 = 18$
$\mathscr{Y}^2 \cos(x)$	1.5×10^{-3}	1.0×10^{-5}	1.7×10^{-6}	3.5×10^{-7}	9.7×10^{-8}	3.3×10^{-8}	1.3×10^{-8}	5.8×10^{-9}
$\dfrac{\mathscr{Y}^2}{3}$	1.2×10^{-3}	9.7×10^{-6}	1.6×10^{-6}	3.4×10^{-7}	9.5×10^{-8}	3.3×10^{-8}	1.3×10^{-8}	5.8×10^{-9}

Figure 1. The AEs for Example 1 when $v_1 = 16$, $\eta(\mathscr{Y}) = \mathscr{Y}^2 \cos(\mathscr{Y})$ and $\eta(\mathscr{Y}) = \dfrac{\mathscr{Y}^2}{3}$ respectively
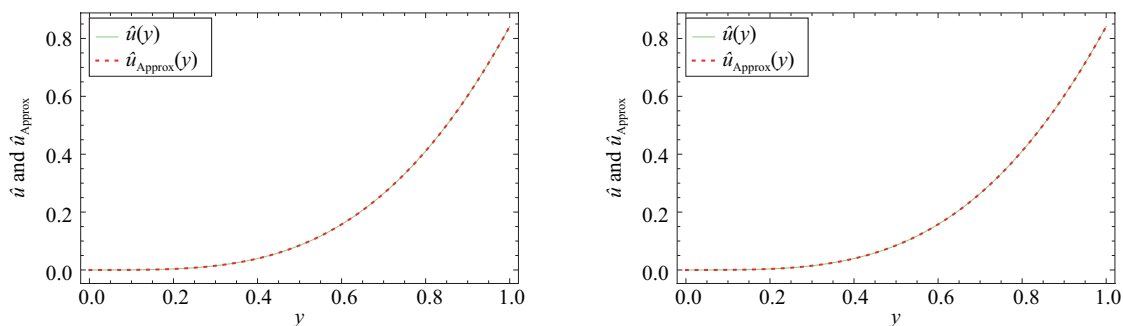

Figure 2. The $\hat{\mathscr{U}}_{\text{Approx}}(\mathscr{Y})$ and $\hat{\mathscr{U}}(\mathscr{Y})$ for Example 1 when $v_2 = 16$ and $\eta(\mathscr{Y}) = \mathscr{Y}^2 \cos(x)$ and $\eta(\mathscr{Y}) = \dfrac{\mathscr{Y}^2}{3}$ respectively

Taking $v_2 = 16$ and $\eta(\mathscr{Y}) = \mathscr{Y}^2 \cos(x)$, we obtain the numerical approximation $\hat{\mathscr{U}}_{\text{Approx}}(\mathscr{Y})$ of Example 1 as:

$$\hat{\mathscr{U}}_{\text{Approx}}(\mathscr{Y}) = -5.55112 \times 10^{-17} + 6.80521 \times 10^{-6}\mathscr{Y} - 0.00123008\mathscr{Y}^2 + 0.13706\mathscr{Y}^3 + 2.55368\mathscr{Y}^4$$

$$-9.41551\mathscr{Y}^5 + 39.9614\mathscr{Y}^6 - 140.491\mathscr{Y}^7 + 380.918\mathscr{Y}^8 - 787.504\mathscr{Y}^9 + 1,232.86\mathscr{Y}^{10} \tag{62}$$

$$-1,446.98\mathscr{Y}^{11} + 1,250.72\mathscr{Y}^{12} - 771.615\mathscr{Y}^{13} + 321.258\mathscr{Y}^{14} - 80.8449\mathscr{Y}^{15} + 9.28482\mathscr{Y}^{16}.$$
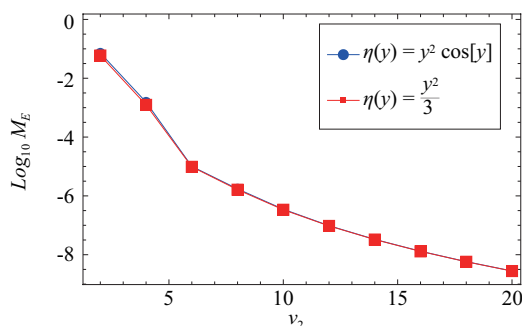
Figure 3. The M_E convergence for Example 1 when $\eta(\mathscr{Y}) = \mathscr{Y}^2 \cos(x)$ and $\eta(\mathscr{Y}) = \dfrac{\mathscr{Y}^2}{3}$ respectively

Taking $v_2 = 16$ and $\eta(\mathscr{Y}) = \dfrac{\mathscr{Y}^2}{3}$, we acquire the numerical outcome $\hat{\mathscr{U}}_{\text{Approx}}(\mathscr{Y})$ of Example 1 as:

$$\hat{\mathscr{U}}_{\text{Approx}}(\mathscr{Y}) = 0. + 6.74469 \times 10^{-6}\mathscr{Y} - 0.00122209\mathscr{Y}^2 + 0.136719\mathscr{Y}^3 + 2.56075\mathscr{Y}^4 - 9.49992\mathscr{Y}^5$$

$$+40.6046\mathscr{Y}^6 - 143.81\mathscr{Y}^7 + 392.96\mathscr{Y}^8 - 818.943\mathscr{Y}^9 + 1,292.59\mathscr{Y}^{10} - 1,529.63\mathscr{Y}^{11} \tag{63}$$

$$+1,333.11\mathscr{Y}^{12} - 829.233\mathscr{Y}^{13} + 348.072\mathscr{Y}^{14} - 88.3007\mathscr{Y}^{15} + 10.2219\mathscr{Y}^{16}.$$

Example 2 Consider the non-linear VDO-FDEs with non-smooth solution:

$$\begin{cases} D_{\mathscr{Y}}^{W_1(\eta(\mathscr{Y}))}\hat{\mathscr{U}}(\mathscr{Y}) - \hat{\mathscr{U}}(\mathscr{Y}) + (\hat{\mathscr{U}}(\mathscr{Y}))^3 = G(\mathscr{Y}), \\ \mathscr{Y}(0) = 0. \end{cases} \tag{64}$$

$G(\mathscr{Y})$ is given from the exact solution $\hat{\mathscr{U}}(\mathscr{Y}) = \mathscr{Y}^{\frac{7}{2}}e^{2\mathscr{Y}^2}$, where $D_{\mathscr{Y}}^{W_1(\eta(\mathscr{Y}))}\hat{\mathscr{U}}(\mathscr{Y}) = \int_0^1 \Gamma(\eta(\mathscr{Y}) - 0.5) D^{\eta(\mathscr{Y})}\hat{\mathscr{U}}(\mathscr{Y}) \, d\eta(\mathscr{Y})$.

We obtain L_∞ with various values of v_2 and and $\eta(\mathscr{Y})$ in Table 2 in this Example 2. Figure 4 represents the AEs of Example 2 when $v_1 = 16$, $\eta(\mathscr{Y}) = 0.9\mathscr{Y}$ and $\eta(\mathscr{Y}) = \mathscr{Y}\sin(\mathscr{Y})$ respectively. Figure 5 compare the exact and approximate solutions when $v_2 = 16$ and $\eta(\mathscr{Y}) = 0.9\mathscr{Y}$ and $\eta(\mathscr{Y}) = \mathscr{Y}\sin(\mathscr{Y})$ respectively. The convergence decay of our technique is shown in Figure 6. The results show that, even by a few points, our technique is more accurate.

Table 2. The MAE of Example 2 with various values of v_2 and $\eta(\mathscr{Y})$

$\eta(\mathscr{Y})$	$v_2 = 4$	$v_2 = 6$	$v_2 = 8$	$v_2 = 10$	$v_2 = 12$	$v_2 = 14$	$v_2 = 16$	$v_2 = 18$
$0.9\mathscr{Y}$	3.2×10^{-1}	2.6×10^{-2}	1.4×10^{-3}	5.4×10^{-5}	1.7×10^{-6}	3.3×10^{-8}	1.4×10^{-8}	6.1×10^{-9}
$\mathscr{Y}\sin(\mathscr{Y})$	3.5×10^{-1}	2.6×10^{-2}	1.3×10^{-3}	5.2×10^{-5}	1.6×10^{-6}	3.2×10^{-8}	1.3×10^{-8}	5.8×10^{-9}
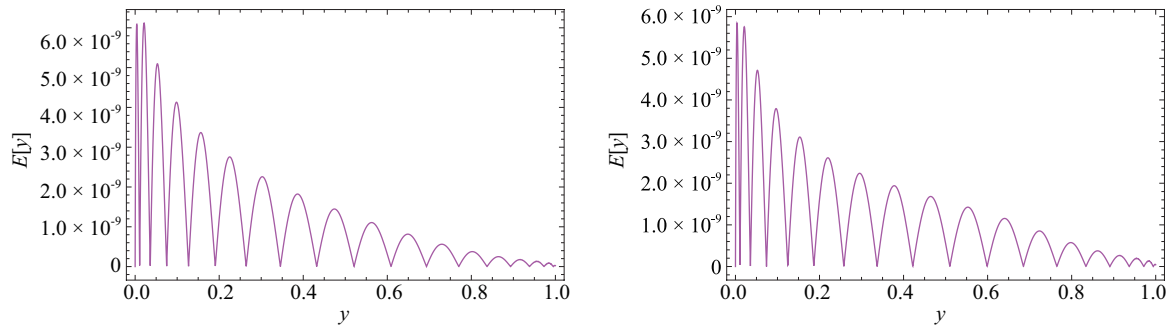
Figure 4. The AEs for Example 2 when $v_1 = 16$, $\eta(\mathscr{Y}) = 0.9\mathscr{Y}$ and $\eta(\mathscr{Y}) = \mathscr{Y}\sin(\mathscr{Y})$ respectively
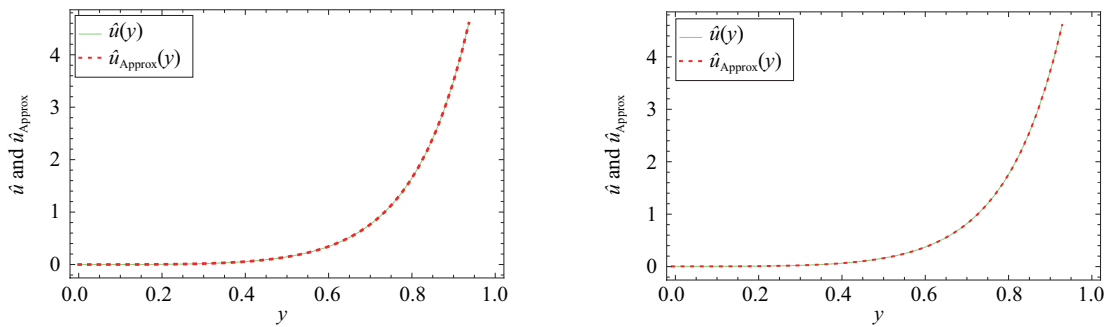

Figure 5. The $\hat{\mathscr{U}}_{\text{Approx}}(\mathscr{Y})$ and $\hat{\mathscr{U}}(\mathscr{Y})$ for Example 2 when $v_2 = 16$ and $\eta(\mathscr{Y}) = 0.9\mathscr{Y}$ and $\eta(\mathscr{Y}) = \mathscr{Y}\sin(\mathscr{Y})$ respectively
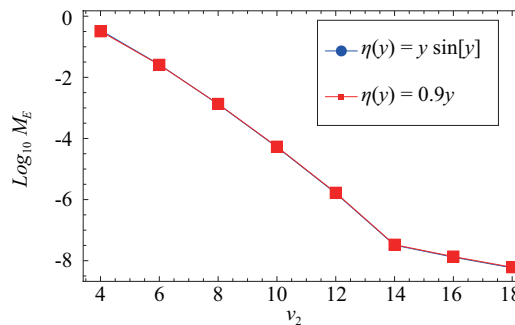

Figure 6. The M_E convergence for Example 2 when $\eta(\mathscr{Y}) = 0.9\mathscr{Y}$ and $\eta(\mathscr{Y}) = \mathscr{Y}\sin(\mathscr{Y})$ respectively

Table 2 shows that the proposed method achieves highly accurate approximations even for moderate values of v_2. The MAE decreases rapidly as v_2 increases, demonstrating the exponential convergence of the method. The two different forms of $\eta(\mathscr{Y})$ produce similar accuracy, indicating the robustness of the technique for different fractional distributions. As shown in Figure 6, the maximum error decays exponentially with increasing v_2, which is a typical characteristic

of spectral collocation methods. Minor differences between the two $\eta(\mathscr{Y})$ choices reflect the influence of the fractional distribution on solution sensitivity. Taking $v_2 = 18$ and $\eta(\mathscr{Y}) = \mathscr{Y}\sin(\mathscr{Y})$, we acquire the numerical outcome $\hat{\mathscr{U}}_{\text{Approx}}(\mathscr{Y})$ of Example 2 as:

$$\hat{\mathscr{U}}_{\text{Approx}}(\mathscr{Y}) = 0. + 3.80936 \times 10^{-6}\mathscr{Y} - 0.000867023\mathscr{Y}^2 + 0.121913\mathscr{Y}^3 + 2.87085\mathscr{Y}^4 - 13.1463\mathscr{Y}^5$$

$$+ 78.7328\mathscr{Y}^6 - 351.038\mathscr{Y}^7 + 1,260.04\mathscr{Y}^8 - 3,510.66\mathscr{Y}^9 + 7,616.62\mathscr{Y}^{10} - 12,817.9\mathscr{Y}^{11}$$

$$\tag{65}$$

$$+ 16,651.\mathscr{Y}^{12} - 16,510.3\mathscr{Y}^{13} + 12,256.5\mathscr{Y}^{14} - 6,590.54\mathscr{Y}^{15} + 2,423.89\mathscr{Y}^{16} - 545.528\mathscr{Y}^{17}$$

$$+ 56.7422\mathscr{Y}^{18}.$$

Taking $v_2 = 18$ and $\eta(\mathscr{Y}) = 0.9\mathscr{Y}$, we acquire the numerical outcome $\hat{\mathscr{U}}_{\text{Approx}}(\mathscr{Y})$ of Example 2 as:

$$\hat{\mathscr{U}}_{\text{Approx}}(\mathscr{Y}) = 0. + 3.93134 \times 10^{-6}\mathscr{Y} - 0.000885176\mathscr{Y}^2 + 0.122798\mathscr{Y}^3 + 2.84965\mathscr{Y}^4 - 12.8479\mathscr{Y}^5$$

$$+ 76.0079\mathscr{Y}^6 - 333.878\mathscr{Y}^7 + 1,182.45\mathscr{Y}^8 - 3,251.98\mathscr{Y}^9 + 6,970.11\mathscr{Y}^{10} - 11,596.2\mathscr{Y}^{11}$$

$$\tag{66}$$

$$+ 14,903.2\mathscr{Y}^{12} - 14,629.9\mathscr{Y}^{13} + 10,759.8\mathscr{Y}^{14} - 5,736.08\mathscr{Y}^{15} + 2,093.09\mathscr{Y}^{16}$$

$$- 467.755\mathscr{Y}^{17} + 48.3607\mathscr{Y}^{18}.$$

Example 3 We consider the non-linear VDO-FDEs:

$$\begin{cases} D_{\mathscr{Y}}^{W_1(\eta(\mathscr{Y}))}\hat{\mathscr{U}}(\mathscr{Y}) - \sqrt{\mathscr{Y}}(\hat{\mathscr{U}}(\mathscr{Y}))^2 = G(\mathscr{Y}), \\ \mathscr{Y}(0) = 0. \end{cases} \tag{67}$$

$G(\mathscr{Y})$ is given from the exact solution $\hat{\mathscr{U}}(\mathscr{Y}) = \mathscr{Y}^2(e^{2\mathscr{Y}} - 1)$, where $D_{\mathscr{Y}}^{W_1(\eta(\mathscr{Y}))}\hat{\mathscr{U}}(\mathscr{Y}) = \int_0^1 \Gamma(\eta(\mathscr{Y}) - 0.5)D^{\eta(\mathscr{Y})}\hat{\mathscr{U}}(\mathscr{Y})d\eta(\mathscr{Y})$.

We obtain L_∞ with various values of v_2 and $\eta(\mathscr{Y})$ in Table 3 in this Example 3. Figure 7 illustrates the AEs of Example 3 when $v_1 = 14$, $\eta(\mathscr{Y}) = \dfrac{\mathscr{Y}\sin(\mathscr{Y})}{3}$ and $\eta(\mathscr{Y}) = \dfrac{\mathscr{Y}}{3}$ respectively. Figure 8 compare the exact and approximate solutions when $v_2 = 16$, $\eta(\mathscr{Y}) = \dfrac{\mathscr{Y}\sin(\mathscr{Y})}{3}$ and $\eta(\mathscr{Y}) = \dfrac{\mathscr{Y}}{3}$ respectively. The convergence decay of our method is illustrated in Figure 9. The findings demonstrate that our method provides improved accuracy even with a small number of data points.

Table 3. The MAE of Example 3 with virous of v_2 and $\eta(\mathscr{Y})$

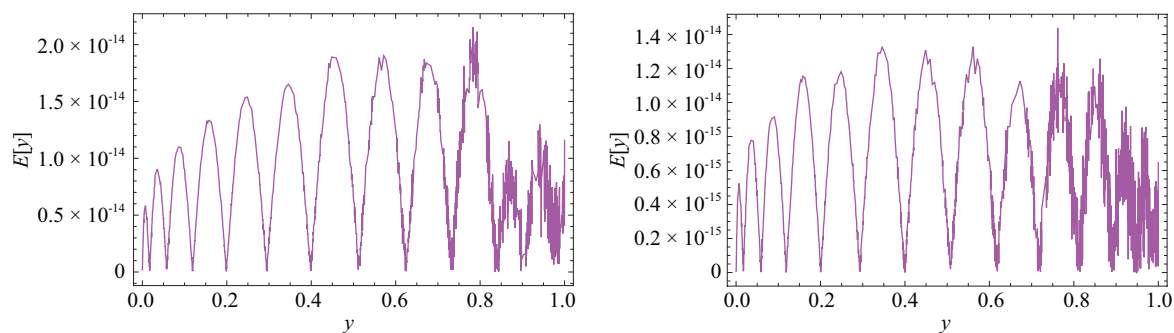| $\eta(\mathscr{Y})$	$v_2 = 2$	$v_2 = 4$	$v_2 = 6$	$v_2 = 8$	$v_2 = 10$	$v_2 = 12$	$v_2 = 14$
$\dfrac{\mathscr{Y}\sin(\mathscr{Y})}{3}$	8.7×10^{-1}	2.1×10^{-2}	2.1×10^{-4}	1.1×10^{-6}	3.7×10^{-9}	8.1×10^{-12}	1.5×10^{-14}
$\dfrac{\mathscr{Y}}{3}$	8.5×10^{-1}	2.1×10^{-2}	2.2×10^{-4}	1.2×10^{-6}	3.9×10^{-9}	8.4×10^{-12}	1.4×10^{-14}

Figure 7. The AEs for Example 3 when $v_1 = 14$, $\eta(\mathscr{Y}) = \dfrac{\mathscr{Y}\sin(\mathscr{Y})}{3}$ and $\eta(\mathscr{Y}) = \dfrac{\mathscr{Y}}{3}$ respectively
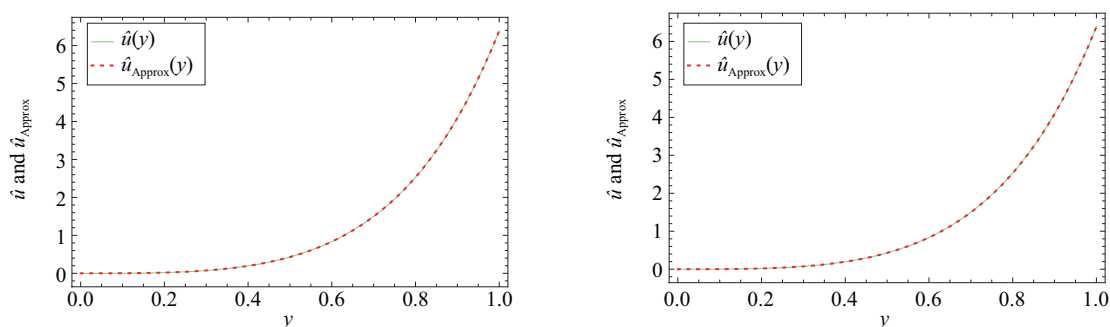

Figure 8. The $\hat{\mathscr{U}}_{\text{Approx}}(\mathscr{Y})$ and $\hat{\mathscr{U}}(\mathscr{Y})$ for Example 3 when $v_2 = 14$ and $\eta(\mathscr{Y}) = \dfrac{\mathscr{Y}\sin(\mathscr{Y})}{3}$ and $\eta(\mathscr{Y}) = \dfrac{\mathscr{Y}}{3}$ respectively
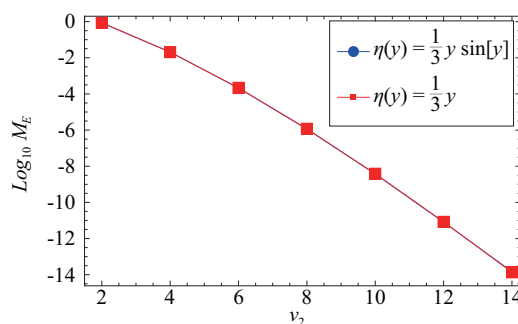

Figure 9. The M_E convergence for Example 3 when $\eta(\mathscr{Y}) = \dfrac{\mathscr{Y}\sin(\mathscr{Y})}{3}$ and $\eta(\mathscr{Y}) = \dfrac{\mathscr{Y}}{3}$ respectively

Taking $v_2 = 14$ and $\eta(\mathscr{Y}) = \dfrac{\mathscr{Y}}{3}$, we acquire the numerical outcome $\hat{\mathscr{U}}_{\text{Approx}}(\mathscr{Y})$ of Example 2 as:

$$\hat{\mathscr{U}}_{\text{Approx}}(\mathscr{Y}) = 0. - 1.70886 \times 10^{-12}\mathscr{Y} + 1.77693 \times 10^{-10}\mathscr{Y}^2 + 2.\mathscr{Y}^3 + 2.\mathscr{Y}^4 + 1.33333\mathscr{Y}^5 + 0.666673\mathscr{Y}^6$$

$$+ 0.266641\mathscr{Y}^7 + 0.0889643\mathscr{Y}^8 + 0.02524\mathscr{Y}^9 + 0.00658141\mathscr{Y}^{10} + 0.00116868\mathscr{Y}^{11} \tag{68}$$

$$+ 0.000454715\mathscr{Y}^{12} - 0.0000270163\mathscr{Y}^{13} + 0.0000278129\mathscr{Y}^{14}.$$

Taking $v_2 = 14$ and $\eta(\mathscr{Y}) = \dfrac{\mathscr{Y}\sin(\mathscr{Y})}{3}$, we acquire the numerical outcome $\hat{\mathscr{U}}_{\mathrm{Approx}}(\mathscr{Y})$ of Example 2 as:

$$\hat{\mathscr{U}}_{\mathrm{Approx}}(\mathscr{Y}) = 0. - 1.55609 \times 10^{-12}\mathscr{Y} + 1.63654 \times 10^{-10}\mathscr{Y}^2 + 2.\mathscr{Y}^3 + 2.\mathscr{Y}^4 + 1.33333\mathscr{Y}^5 + 0.666673\mathscr{Y}^6$$

$$+ 0.266642\mathscr{Y}^7 + 0.0889617\mathscr{Y}^8 + 0.0252446\mathscr{Y}^9 + 0.00657583\mathscr{Y}^{10} + 0.00117331\mathscr{Y}^{11} \qquad (69)$$

$$+ 0.000452205\mathscr{Y}^{12} - 0.0000262183\mathscr{Y}^{13} + 0.0000276999\mathscr{Y}^{14}.$$

Example 4 Consider the non-linear VDO-FDEs with non-smooth solution with the boundary conditions:

$$\begin{cases} D_{\mathscr{Y}}^{W_1(\eta(\mathscr{Y}))}\hat{\mathscr{U}}(\mathscr{Y}) - 20\hat{\mathscr{U}}(\mathscr{Y}) + 30(\hat{\mathscr{U}}(\mathscr{Y}))^3 = G(\mathscr{Y}), \\ \mathscr{Y}(0) = 0, \\ \mathscr{Y}(2) = 8\sqrt{2}. \end{cases} \qquad (70)$$

$G(\mathscr{Y})$ is given from the exact solution $\hat{\mathscr{U}}(\mathscr{Y}) = \mathscr{Y}^{\frac{7}{2}}$, where $D_{\mathscr{Y}}^{W_1(\eta(\mathscr{Y}))}\hat{\mathscr{U}}(\mathscr{Y}) = \int_0^1 \Gamma(\eta(\mathscr{Y}) - 0.5)D^{\eta(\mathscr{Y})}\hat{\mathscr{U}}(\mathscr{Y})$ $d\eta(\mathscr{Y})$.

Table 4. The MAE of Example 4 with various values of v_2 and $\eta(\mathscr{Y}) = \mathscr{Y}\sin(\mathscr{Y})$

v_2	MAE
2	8.729×10^{-1}
4	7.816×10^{-2}
6	3.896×10^{-3}
8	1.529×10^{-4}
10	6.484×10^{-6}
12	5.238×10^{-7}
14	1.113×10^{-7}
16	3.702×10^{-8}
18	1.450×10^{-8}
20	6.286×10^{-9}

Table 4 demonstrates that the proposed spectral technique maintained high accuracy even when applied to this nonlinear problem with a non-smooth solution. The MAE values decrease exponentially as v_2 increases, confirming the spectral convergence behavior of the method. The results further show that the technique effectively handles nonlinearities of cubic order without stability deterioration or loss of accuracy. As illustrated in Figure 10, the absolute errors remain uniformly small across the entire domain, while Figure 11 indicates a clear exponential decay trend with increasing collocation points. These findings confirm the robustness and computational efficiency of the proposed approach, even for complex fractional operators and non-smooth boundary behaviors.
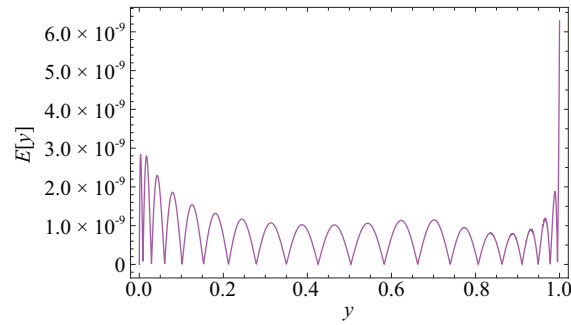
Figure 10. The AEs for Example 4 when $v_1 = 20$, $\eta(\mathscr{Y}) = \mathscr{Y}\sin(\mathscr{Y})$
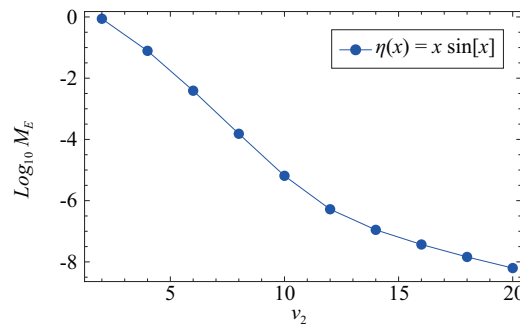

Figure 11. The M_E convergence for Example 4 when $\eta(\mathscr{Y}) = \mathscr{Y}\sin(\mathscr{Y})$

Example 5 We consider time nonlinear VDO-FDEs,

$$\begin{cases} D_t^{\omega(\eta(\chi))}\hat{\mathscr{U}}(\mathscr{Y},\,\chi) - \dfrac{\partial^2 \hat{\mathscr{U}}(\mathscr{Y},\,\chi)}{\partial \mathscr{Y}^2} - (\hat{\mathscr{U}}(\mathscr{Y},\,\chi))^3 = G(\mathscr{Y},\,\chi), \\ \hat{\mathscr{U}}(\mathscr{Y},\,0) = 0, \\ \hat{\mathscr{U}}(0,\,\chi) = \chi^{\frac{1}{2}}, \qquad \hat{\mathscr{U}}(1,\,\chi) = \chi^{\frac{1}{2}}\cos(1), \end{cases} \tag{71}$$

where the exact solution $\hat{\mathscr{U}}(\mathscr{Y},\,\chi) = \chi^{\frac{1}{2}}\cos(\mathscr{Y})$ and $\eta(\chi) = \dfrac{\chi^3}{2}$.

While $D_\chi^{\omega(\eta(\chi))}\hat{\mathscr{U}}(\mathscr{Y},\,\chi) = \int_0^1 \Gamma(4 - \eta(\chi))D^{\eta(\chi)}\hat{\mathscr{U}}(\mathscr{Y},\,\chi)d\eta(\chi)$.

We obtain L_∞ for different $\mathscr{M}$ and $\mathscr{N}$ values in Table 5 in this Example 5. Figure 12 represents the $\mathscr{Y}$-direction, and χ-direction of Example 5. Figure 13 shows the AEs for Example 5. The convergence decay of our technique is shown in Figure 14. The results show that even by a few points our technique is more accurate. Table 5 demonstrates that the proposed method achieves high accuracy even with a small number of collocation points. As $\mathscr{N}$ and $\mathscr{M}$ increase, the MAE decreases rapidly, confirming the spectral convergence of the method. Figures 12-14 illustrate the effectiveness of the proposed approach in capturing the non-linear and time-dependent features of the solution. The rapid decay of the absolute error and the MAE with increasing collocation points indicates that even a relatively coarse discretization accurately approximates the exact solution.

Table 5. The MAE for Example 5

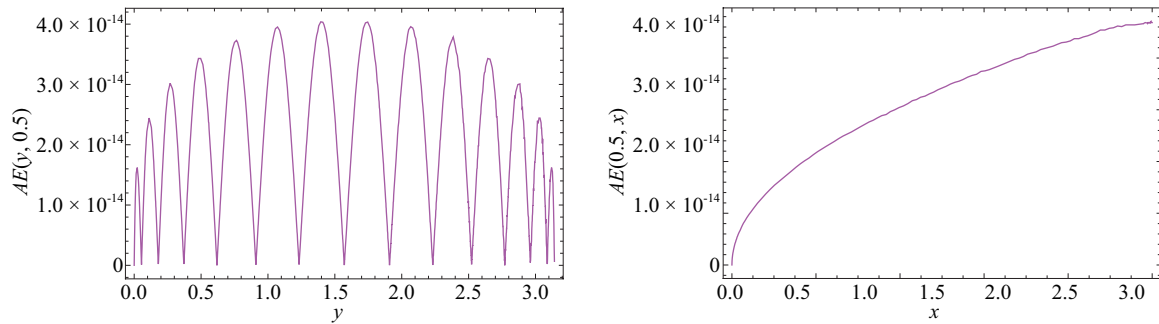| $(\mathcal{N}, \mathcal{M})$	$(2, 2)$	$(4, 4)$	$(6, 6)$	$(8, 8)$	$(10, 10)$	$(12, 12)$	$(14, 14)$
MAE	2.10×10^{-1}	7.10×10^{-3}	1.02×10^{-4}	8.75×10^{-7}	4.92×10^{-9}	1.93×10^{-11}	5.55×10^{-14}

Figure 12. $\mathcal{Y}$ and χ-direction curve of the AEs Example 5 when $\mathcal{N} = \mathcal{M} = 14$ and $\eta(\chi) = \dfrac{\chi^3}{2}$
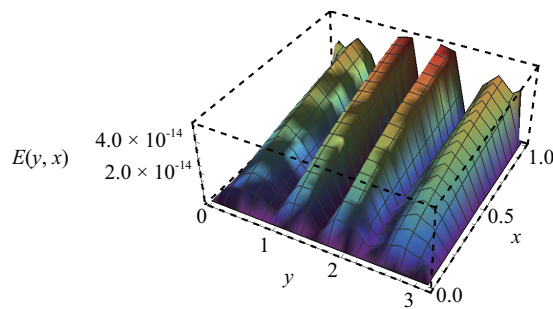

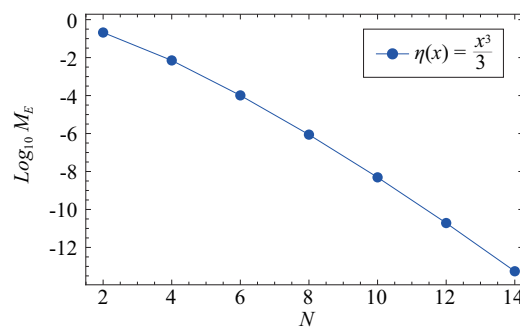**Figure 13.** AEs for Example 5 for $\mathcal{N} = \mathcal{M} = 14$

Figure 14. MAE convergence for Example 5 for difference of $\mathcal{N}, \mathcal{M}$

Example 6 We consider time nonlinear VDO-FDEs,

$$
\begin{cases}
D_t^{\omega(\eta(\chi))}\hat{\mathscr{U}}(\mathscr{Y},\chi) - \dfrac{\partial^2 \hat{\mathscr{U}}(\mathscr{Y},\chi)}{\partial \mathscr{Y}^2} - (\hat{\mathscr{U}}(\mathscr{Y},\chi))^2 = G(\mathscr{Y},\chi), \\[2mm]
\hat{\mathscr{U}}(\mathscr{Y},0) = 0, \\[2mm]
\hat{\mathscr{U}}(0,\chi) = 0, \qquad \hat{\mathscr{U}}(1,\chi) = \chi^{\frac{1}{2}}\sin(1),
\end{cases}
\tag{72}
$$

where the exact solution $\hat{\mathscr{U}}(\mathscr{Y},\chi) = \chi^{\frac{1}{2}}\sin(\mathscr{Y})$ and $\eta(\chi) = \dfrac{\chi^2}{3}$.

While $D_\chi^{\omega(\eta(\chi))}\hat{\mathscr{U}}(\mathscr{Y},\chi) = \int_0^1 \Gamma(4 - \eta(\chi))D^{\eta(\chi)}\hat{\mathscr{U}}(\mathscr{Y},\chi)d\eta(\chi)$.

We obtain L_∞ for different $\mathscr{N}$ and $\mathscr{M}$ values in Table 6 in this Example 6, while Table 7 displays AEs with $\eta(\chi) = \dfrac{t^2}{3}$. Figure 15 illustrates the $\mathscr{Y}$-direction, and χ-direction of Example 6. Figure 16 shows the AEs for Example 6 for $\mathscr{N} = \mathscr{M} = 14$ with $\eta(\chi) = \dfrac{t^2}{3}$. The convergence decay of our technique is shown in Figure 17. The results show that even by a few points our technique is more accurate. Figures 15-17 illustrate the effectiveness of the proposed method in accurately resolving the time-dependent nonlinear VDO-FDE. The rapid decay of absolute error and MAE with increasing collocation points indicates the spectral accuracy of the method. This demonstrates that the approach provides highly accurate solutions even with a relatively coarse discretization.

Table 6. The MAE for Example 6

$(\mathscr{N},\mathscr{M})$	(2, 2)	(4, 4)	(6, 6)	(8, 8)	(10, 10)	(12, 12)	(14, 14)
MAE	8.22×10^{-2}	1.81×10^{-3}	1.54×10^{-5}	1.02×10^{-7}	4.76×10^{-10}	1.53×10^{-12}	4.22×10^{-15}

Table 7. L_∞ for Example 6 with various values of $\mathscr{Y}$, χ, $\mathscr{N}$, and $\mathscr{M}$

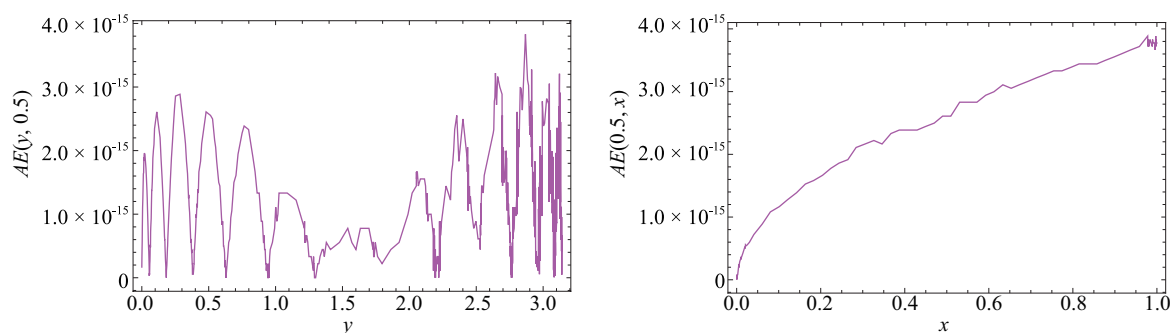| $(\mathscr{Y},\chi)$	$\mathscr{N} = \mathscr{M} = 12$	$\mathscr{N} = \mathscr{M} = 14$
(0.1, 0.1)	2.4807×10^{-13}	1.0894×10^{-15}
(0.2, 0.2)	4.6731×10^{-13}	5.5511×10^{-16}
(0.3, 0.3)	5.7590×10^{-13}	2.0262×10^{-15}
(0.4, 0.4)	9.2640×10^{-13}	6.9389×10^{-16}
(0.5, 0.5)	9.0594×10^{-14}	2.6090×10^{-15}
(0.6, 0.6)	8.9195×10^{-13}	1.0547×10^{-15}
(0.7, 0.7)	1.0666×10^{-12}	1.8874×10^{-15}
(0.8, 0.8)	4.0001×10^{-13}	2.6645×10^{-15}
(0.9, 0.9)	4.7573×10^{-13}	7.7716×10^{-16}

Figure 15. $\mathscr{Y}$ and χ-direction curve of the AEs Example 6 when $\mathscr{N} = \mathscr{M} = 14$ and $\eta(\chi) = \dfrac{\chi^2}{3}$
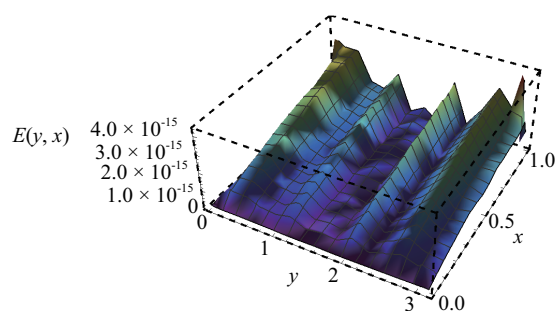
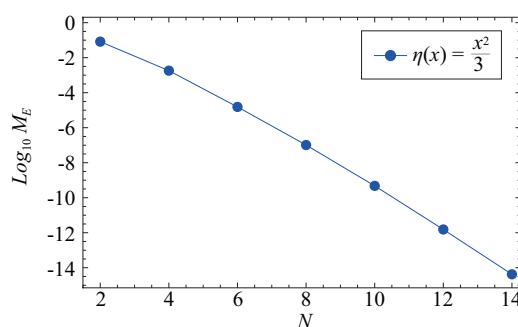**Figure 16.** AEs for Example 6 for $\mathscr{N} = \mathscr{M} = 14$

Figure 17. MAE convergence for Example 6 for difference of $\mathscr{N}$, $\mathscr{M}$

Example 7 We consider time Distributed-Order Fractional Differential Equations (DO-FDEs),

$$
\begin{cases}
D_t^{\omega(\eta(\chi))}\hat{\mathscr{U}}(\mathscr{Y}, \chi) - \dfrac{\partial^2 \hat{\mathscr{U}}(\mathscr{Y}, \chi)}{\partial \mathscr{Y}^2} = G(\mathscr{Y}, \chi), \\
\hat{\mathscr{U}}(\mathscr{Y}, 0) = 0, \\
\hat{\mathscr{U}}(0, \chi) = 0, \qquad \hat{\mathscr{U}}(1, \chi) = 0,
\end{cases}
\tag{73}
$$

where the exact solution $\hat{\mathscr{U}}(\mathscr{Y}, \chi) = \chi^{\frac{3}{2}}\mathscr{Y}^2(1-\mathscr{Y})^4$.

While $D_\chi^{\omega(\eta(\chi))}\hat{\mathscr{U}}(\mathscr{Y}, \chi) = \int_0^1 \Gamma\left(\dfrac{5}{2} - \eta(\chi)\right) D^{\eta(\chi)}\hat{\mathscr{U}}(\mathscr{Y}, \chi)d\eta(\chi)$.

Table 8. The MAE for Example 7

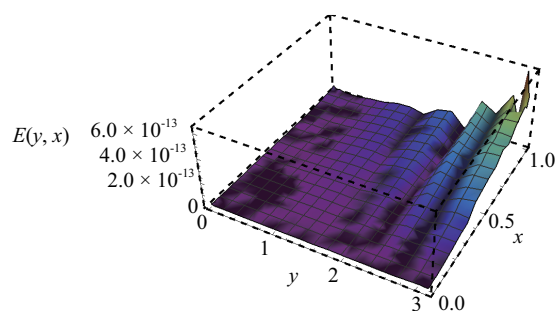| $(\mathscr{N}, \mathscr{M})$	(6, 6)	(7, 7)	(8, 8)	(9, 9)	(10, 10)
MAE in [37]	4×10^{-6}	2.43×10^{-6}	1.57×10^{-6}	1.07×10^{-6}	7.57×10^{-7}
MAE	4.29×10^{-10}	6.45×10^{-12}	1.60×10^{-13}	5.68×10^{-14}	4.76×10^{-14}

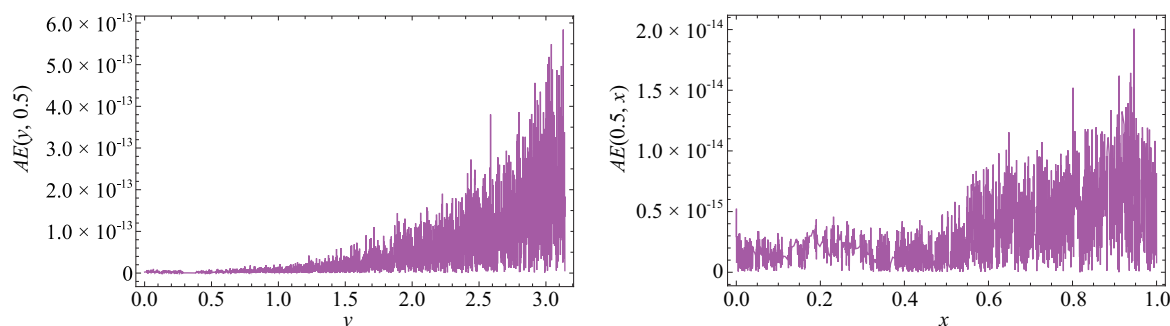**Figure 18.** AEs for Example 7 for $\mathcal{N} = \mathcal{M} = 10$

Figure 19. $\mathscr{Y}$ and χ-direction curve of the AEs Example 7 when $\mathcal{N} = \mathcal{M} = 10$

Table 8 presents the Mean Absolute Error (MAE) for Example 7 and compares the results with those reported in [37]. It is evident that the proposed method achieves significantly higher accuracy, with errors reduced by several orders of magnitude for all tested grid sizes. The rapid decay of the MAE as $(\mathcal{N}, \mathcal{M})$ increase confirms the exponential convergence behavior typical of spectral approaches. Figures 18-19 illustrate the absolute error distribution and directional profiles of the approximate solution, showing smooth and stable behavior across both spatial and temporal directions. These results demonstrate that the present scheme not only outperforms existing methods in accuracy but also maintains robustness and efficiency for nonlinear variable-order fractional differential equations.

6. Conclusion

Our primary objective is to improve spectral algorithms for solving non-linear VDO-FDEs using the SL-GL-C method, particularly focusing on non-smooth solutions. These new algorithms are developed by transforming the mentioned problems into a system of algebraic equations. In addition, we solve time nonlinear VDO-FDEs with initial and boundary conditions using FSL-GL and SC-GR. The time nonlinear VDO-FDEs are represented by a decreased sequence of SLPs, and SCP. The residuals of the equations at the FSL-GL and SC-GR quadrature points are calculated, resulting in a system of algebraic equations to be solved. Then, we have included numerical examples that demonstrate for assessing the accuracy and practicality of the current algorithms. The comparisons provided show the accuracy and effectiveness of the spectral collection method. Examples that demonstrate a concept or principle.

Conflict of interest

The authors declare no conflict of interest.

References

[1] Doha EH, Bhrawy AH, Abdelkawy MA, Hafez RM. A Jacobi collocation approximation for nonlinear coupled viscous Burgers' equation. *Central European Journal of Physics*. 2014; 12: 111-122.

[2] Bhrawy A, Abdelkawy M, Alzahrani A, Baleanu D, Alzahrani E. A Chebyshev-Laguerre-Gauss-Radau collocation scheme for solving a time fractional sub-diffusion equation on a semi-infinite domain. *Proceedings of the Romanian Academy-Series A: Mathematics, Physics, Technical Sciences, Information Science*. 2015; 16(4): 490-498.

[3] Metzler R, Klafter J. The random walk's guide to anomalous diffusion: A fractional dynamics approach. *Physics Reports*. 2000; 339(1): 1-77.

[4] Bhrawy AH, Alhuthali MS, Abdelkawy MA. New solutions for $(1 + 1)$-dimensional and $(2 + 1)$-dimensional Ito equations. *Mathematical Problems in Engineering*. 2012; 2012(1): 537930.

[5] Azar AT, Radwan AG, Vaidyanathan S. *Fractional Order Systems: Optimization, Control, Circuit Realizations and Applications*. Amsterdam, NL: Academic Press; 2018.

[6] Kilbas AA, Srivastava HM, Trujillo JJ. *Theory and Applications of Fractional Differential Equations*. Amsterdam, NL: Elsevier; 2006.

[7] Mantegna RN, Stanley HE. *Introduction to Econophysics: Correlations and Complexity in Finance*. Cambridge, UK: Cambridge University Press; 1999.

[8] Skovranek T, Despotovic V. Signal prediction using fractional derivative models. In: *Volume 8 Applications in Engineering, Life and Social Sciences, Part B*. Berlin, Boston: De Gruyter; 2019. p.179-206.

[9] Maya-Franco D, Martínez-Guerrero E, Sun GH, Dong SH. Exploring quantum information entropy in double hyperbolic potentials under the fractional Schrödinger framework. *International Journal of Quantum Chemistry*. 2025; 125(15): e70086.

[10] Santana-Carrillo R, Maya-Franco D, Sun GH, Dong SH. Shannon and Fisher entropy for a new class of single hyperbolic potentials in fractional Schrödinger equation. *International Journal of Quantum Chemistry*. 2025; 125(7): e70024.

[11] Santana-Carrillo R, Peto JV, Sun GH, Dong SH. Quantum information entropy for a hyperbolic double well potential in the fractional Schrödinger equation. *Entropy*. 2023; 25(7): 988.

[12] Rabiei K, Razzaghi M. Fractional-order Boubaker wavelets method for solving fractional Riccati differential equations. *Applied Numerical Mathematics*. 2021; 168: 221-234.

[13] Yuttanan B, Razzaghi M, Vo TN. Fractional-order generalized Legendre wavelets and their applications to fractional Riccati differential equations. *International Journal of Nonlinear Sciences and Numerical Simulation*. 2023; 24(1): 57-69.

[14] Doha EH, Abdelkawy M, Baleanu D. Approximate solutions for solving nonlinear variable-order fractional Riccati differential equations. *Nonlinear Analysis: Modelling and Control*. 2019; 24(2): 176-188.

[15] Momani S, Djeddi N, Al-Smadi M, Al-Omari S. Numerical investigation for Caputo-Fabrizio fractional Riccati and Bernoulli equations using iterative reproducing kernel method. *Applied Numerical Mathematics*. 2021; 170: 418-434.

[16] Tvyordyj D. Hereditary Riccati equation with fractional derivative of variable order. *Journal of Mathematical Sciences*. 2021; 253: 564-572.

[17] Sadek L, Samei ME, Hashemi MS. The Galerkin Mittag-Leffler method for solving fractional optimal control problems with inequality constraints. *Mathematics and Computers in Simulation*. 2025; 240: 191-207.

[18] Hashemi MS, Ashpazzadeh E, Moharrami M, Lakestani M. Fractional order Alpert multiwavelets for discretizing delay fractional differential equation of pantograph type. *Applied Numerical Mathematics*. 2021; 170: 1-13.

[19] Delzanno GL. Multi-dimensional, fully-implicit, spectral method for the Vlasov-Maxwell equations with exact conservation laws in discrete form. *Journal of Computational Physics*. 2015; 301: 338-356.

[20] Chen Y, Zhou J. Error estimates of spectral Legendre-Galerkin methods for the fourth-order equation in one dimension. *Applied Mathematics and Computation*. 2015; 268: 1217-1226.

[21] Abdelkawy M, Amin A, Lopes AM. Fractional-order shifted Legendre collocation method for solving non-linear variable-order fractional Fredholm integro-differential equations. *Computational and Applied Mathematics*. 2022; 41(1): 1-21.

[22] Amin AZ, Lopes AM, Hashim I. A Chebyshev collocation method for solving the non-linear variable-order fractional Bagley-Torvik differential equation. *International Journal of Nonlinear Sciences and Numerical Simulation*. 2022; 24(5): 1613-1630.

[23] Abd-Elhameed WM, Youssri YH. New formulas of the high-order derivatives of fifth-kind Chebyshev polynomials: Spectral solution of the convection-diffusion equation. *Numerical Methods for Partial Differential Equations*. 2024; 40(2): e22756.

[24] Amin A, Abdelkawy M, Amin A, Lopes AM, Alluhaybi A, Hashim I. Legendre-Gauss-Lobatto collocation method for solving multi-dimensional systems of mixed Volterra-Fredholm integral equations. *AIMS Mathematics*. 2023; 8(9): 20871-20891.

[25] Tedjani AH, Amin AZ, Abdel-Aty AH, Abdelkawy MA, Mahmoud M. Legendre spectral collocation method for solving nonlinear fractional Fredholm integro-differential equations with convergence analysis. *AIMS Mathematics*. 2024; 9(4): 7973-8000.

[26] Magdy E, Abd-Elhameed WM, Youssri YH, Moatimid GM, Atta AG. A potent collocation approach based on shifted gegenbauer polynomials for nonlinear time fractional Burgers' equations. *Contemporary Mathematics*. 2023; 4(4): 647-665.

[27] Amin AZ, Abdelkawy MA, Soluma EM, Babatin MM. A space-time spectral approximation for solving two dimensional variable-order fractional convection-diffusion equations with nonsmooth solutions. *International Journal of Modern Physics C*. 2024; 35(7): 2450088.

[28] Ezz-Eldien SS. On solving systems of multi-pantograph equations via spectral tau method. *Applied Mathematics and Computation*. 2018; 321: 63-73.

[29] Doha EH, Abdelkawy MA, Amin AZ, Baleanu D. Shifted Jacobi spectral collocation method with convergence analysis for solving integro-differential equations and system of integro-differential equations. *Nonlinear Analysis: Modelling and Control*. 2019; 24(3): 332-352.

[30] Ahmed HM, Hafez RM, Abd-Elhameed WM. A computational strategy for nonlinear time-fractional generalized Kawahara equation using new eighth-kind Chebyshev operational matrices. *Physica Scripta*. 2024; 99(4): 045250.

[31] Youssri YH, Abd-Elhameed WM. Numerical spectral Legendre-Galerkin algorithm for solving time fractional telegraph equation. *Romanian Journal of Physics*. 2018; 63(107): 1-16.

[32] Doha EH, Abd-Elhameed WM. Efficient spectral ultraspherical-dual-Petrov-Galerkin algorithms for the direct solution of $(2n + 1)$ th-order linear differential equations. *Mathematics and Computers in Simulation*. 2009; 79(11): 3221-3242.

[33] Doha EH, Abd-Elhameed WM, Youssri YH. Efficient spectral-Petrov-Galerkin methods for the integrated forms of third-and fifth-order elliptic differential equations using general parameters generalized Jacobi polynomials. *Applied Mathematics and Computation*. 2012; 218(15): 7727-7740.

[34] Doha EH, Abdelkawy MA, Amin AZM, Lopes AM. Shifted Jacobi-Gauss-collocation with convergence analysis for fractional integro-differential equations. *Communications in Nonlinear Science and Numerical Simulation*. 2019; 72: 342-359.

[35] Doha EH, Abdelkawy MA, Amin AZM, Lopes AM. A space-time spectral approximation for solving nonlinear variable-order fractional sine and Klein-Gordon differential equations. *Computational and Applied Mathematics*. 2018; 37(5): 6212-6229.

[36] Canuto C, Hussaini MY, Quarteroni A, Zang TA. *Spectral Methods: Fundamentals in Single Domains*. Berlin, Heidelberg: Springer; 2007.

[37] Pourbabaee M, Saadatmandi A. A novel Legendre operational matrix for distributed order fractional differential equations. *Applied Mathematics and Computation*. 2019; 361: 215-231.